EPMA Journal (2023) 14:307–328
https://doi.org/10.1007/s13167-023-00320-w

RESEARCH

Identification of potential necroinflammation-associated necroptosis-related biomarkers for delayed graft function and renal allograft failure: a machine learning-based exploration in the framework of predictive, preventive, and personalized medicine

Qing Bi[1,2] · Ji-Yue Wu[1,2] · Xue-Meng Qiu[1,2,3] · Yu-Qing Li[1,2] · Yu-Yao Yan[4] · Ze-Jia Sun[1,2] · Wei Wang[1,2]

Received: 6 January 2023 / Accepted: 7 April 2023 / Published online: 28 April 2023

Abstract

Delayed graft function (DGF) is one of the key post-operative challenges for a subset of kidney transplantation (KTx) patients. Graft survival is significantly lower in recipients who have experienced DGF than in those who have not. Assessing the risk of chronic graft injury, predicting graft rejection, providing personalized treatment, and improving graft survival are major strategies for predictive, preventive, and personalized medicine (PPPM/3PM) to promote the development of transplant medicine. However, since PPPM aims to accurately identify disease by integrating multiple omics, current methods to predict DGF and graft survival can still be improved. Renal ischemia/reperfusion injury (IRI) is a pathological process experienced by all KTx recipients that can result in varying occurrences of DGF, chronic rejection, and allograft failure depending on its severity. During this process, a necroinflammation-mediated necroptosis-dependent secondary wave of cell death significantly contributes to post-IRI tubular cell loss. In this article, we obtained the expression matrices and corresponding clinical data from the GEO database. Subsequently, nine differentially expressed necroinflammation-associated necroptosis-related genes (NiNRGs) were identified by correlation and differential expression analysis. The subtyping of post-KTx IRI samples relied on consensus clustering; the grouping of prognostic risks and the construction of predictive models for DGF (the area under the receiver operating characteristic curve (AUC) of the internal validation set and the external validation set were 0.730 and 0.773, respectively) and expected graft survival after a biopsy (the internal validation set's 1-year AUC: 0.770; 2-year AUC: 0.702; and 3-year AUC: 0.735) were based on the least absolute shrinkage and selection operator regression algorithms. The results of the immune infiltration analysis showed a higher infiltration abundance of myeloid immune cells, especially neutrophils, macrophages, and dendritic cells, in the cluster A subtype and prognostic high-risk groups. Therefore, in the framework of PPPM, this work provides a comprehensive exploration of the early expression landscape, related pathways, immune features, and prognostic impact of NiNRGs in post-KTx patients and assesses their capabilities as.

- predictors of post-KTx DGF and graft loss,
- targets of the vicious loop between regulated tubular cell necrosis and necroinflammation for targeted secondary and tertiary prevention, and
- references for personalized immunotherapy.

Keywords Predictive preventive personalized medicine (PPPM/3PM) · Kidney transplantation (KTx) · Ischemia/reperfusion injury (IRI) · Acute kidney injury (AKI) · Delayed graft function (DGF) · Tubular cell death · Necroinflammation · Necroptosis · Graft failure · Graft rejection · Disease severity · Prognosis prediction · Individual outcomes · Secondary prevention · Tertiary prevention

Qing Bi, Ji-Yue Wu and Xue-Meng Qiu contributed equally to thiswork.

Extended author information available on the last page of the article

Introduction

Current situation and challenges in the post-KTx complication management under PPPM

As a life-saving therapy, kidney transplantation (KTx) is the established treatment of choice for patients with end-stage renal disease (ESRD) who are suitable for operation. The increased demand for KTx has driven the development of kidney transplant medicine. According to data from the World Health Organization (WHO) Global Observatory on Donation and Transplantation (GODT) in 2021, the yearly global total kidney transplants per million population were 92,532, representing a 14.3% increase compared to the previous year [1]. While the upward trend in the total number of yearly kidney transplants has fluctuated in recent years due to the impact of the COVID-19 pandemic [2], it has risen by approximately 20% in just a decade from 2012 to 2021 [3]. Consequently, the pressure of post-KTx complication management has increased. Delayed graft function (DGF), which is usually defined as the need for dialysis during the first week after KTx, is the major post-operative complication [4, 5]. The rate of DGF in living donor transplants ranges from about 4 to 10%, while 29–38% of deceased-donor KTx recipients are estimated to be complicated by DGF [6–8]. Particularly in recent years, as the proportion of donation after cardiac-death (DCD) donors has increased [9], the DGF rate has increased from 24.4 to 42.5% compared to KTx with donation after brain-death (DBD) donors [10]. The worse outcome relevance of KTx patients who have experienced DGF is mainly reflected in renal dysfunction, graft loss, rejection, and mortality [11, 12]. Therefore, early prediction and targeted intervention are especially important.

Predictive preventive personalized medicine (PPPM) is a future-oriented healthcare strategy that aims to continuously incorporate new biotechnologies to accurately predict diseases, improve preventive measures, and create personalized therapies [13, 14]. Previous medical practice has been to treat symptoms as they arise, which has led to limited improvement in the prognosis for some diseases, especially for diabetes, cardiovascular disease, and cerebrovascular disease. The advent of PPPM has led to a shift in medical treatment from reactive medicine to predictive diagnosis and targeted intervention [13]. In recent years, the PPPM model has been widely proposed for health monitoring and the prevention and precision medicine of many diseases, including cancers, diabetes and its complications, vascular function and lesions, and oral lesions [14–19]. The development of regenerative medicine was also strongly advanced by PPPM; it is dedicated to optimizing the current situation of organ transplantation in the following aspects [13]:

- donor–recipient matching,
- assessing individual risk for chronic graft injury,
- predicting allograft rejection, and
- establishing algorithms for personalized immunosuppressive therapy.

While KTx for ESRD patients is a delayed treatment under the paradigm and expectation of PPPM, the concept of primary, secondary, and tertiary prevention is also applicable to the management of post-KTx complications when we consider KTx as a new beginning of life for those patients. However, the application of PPPM in KTx medicine is clearly limited compared to those diseases we have mentioned before. While PPPM has helped clinicians to better match donors and recipients, early prediction and prevention of post-KTx complications, such as DGF and graft loss, are not enough. The previous biopsy-based pathology scores were apparently a delayed diagnosis, which did not meet the requirements of PPPM [13]. Furthermore, some previous predictive models had limited ability to predict DGF [20]. Indeed, researchers have been constantly trying to find biomarkers to diagnose or predict renal allograft dysfunction, and some of the findings have had varying degrees of success in the preclinical and clinical stages [21, 22]. However, there is growing evidence that a perfect single marker may not exist [13]. Within the framework of PPPM, the improvement of multi-stage and multi-omic diagnosis is the key to achieving targeted prevention and personalized treatment, avoiding unnecessary medication, and reducing the morbidity of post-KTx complications. Bioinformatics has long been considered an enabler for the advances in PPPM [23]. In recent years, the rapid development of this discipline has also demonstrated the great potential of improving the post-KTX PPPM; its application in KTx to identify biomarkers is consequently necessary.

IRI, a contributor to DGF and graft loss

Ischemia/reperfusion injury (IRI), as a common cause of acute kidney injury (AKI), is a mostly inevitable pathological process in patients undergoing KTx or other types of kidney operations, such as partial nephrectomy [24]. Severe IRI often leads to a higher tendency of developing severe DGF, which can result in an unpromising prognosis such as long-term chronic rejection or even graft loss [4, 5, 25]. However, IRI-induced AKI (IRI-AKI) and the possible subsequent occurrence of DGF remain critical concerns, with a limited comprehensive understanding of their mechanisms, reliable predictive methods, and alternative therapeutic options [26, 27].

IRI-induced renal tubular cell death

Tubular cell death is an important characteristic of AKI. Multiple regulated cell deaths (RCDs), including apoptosis and regulated necroses (RNs) via ferroptosis, pyroptosis, necroptosis, and NETosis, have been reported to be involved in the loss of tubular cells during IRI-, sepsis-, or folic acid (FA)-induced AKI [28–30]. As research into AKI has progressed, scholars have increasingly focused on the timing of the occurrence of these RCDs, the position they occupy, and the intersections. Necroptosis, characterized by cell swelling and rupture as well as the increased release of DAMPs and pro-inflammatory cytokines, is an inflammation-associated RN driven by activated RIPK1or other receptor-interacting protein kinase (RIP) homotypic interaction motif (RHIM) domain-containing proteins (such as TRIF or ZBP1) via the sequential phosphorylation of downstream RIPK3 and MLKL [31]. Martin-Sanchez et al. revealed that, during the initial 48 h, primitive insult-induced RNs—mainly ferroptosis—contribute to the first wave of tubular cell death [32]. Ferroptotic and other regulated necrotic cells trigger inflammation and cytokine release through the release of intracellular components as well as damage-associated molecular patterns (DAMPs); this is called necroinflammation, and it leads to secondary cell death, especially necroptosis, thus engendering a vicious cycle [33–35] (Fig. 1). On the other hand, ferroptosis, necroptosis, and apoptosis are substitutable; inhibition in one pathway causes cells to be sensitive to death through another pathway [33, 34, 36]. While early blockade of the necroptosis-related pathway lacks a significant protective effect on renal function in the first 48 h, it is effective in preventing vicious cycling and improving the prognosis of renal function [33, 34].

Working hypothesis

Recently, necroptosis has been reported to be implicated in the evolution of cardio-cerebrovascular, autoimmune, inflammatory, infectious, and malignant diseases, as well as AKI and IRI [37, 38]. However, a comprehensive description of necroptosis-related genes (NRGs), especially necroinflammation-associated NRGs (NiNRGs), with regard to the expression at the early stage of IRI-AKI is lacking. Thanks to the rapid development of sequencing technologies, bioinformatics analysis integrating machine learning algorithms has promoted the identification of disease biomarkers [39, 40], providing opportunities for advancing early prediction, precise diagnosis, targeted intervention, and personalized treatment of diseases in the framework of PPPM [16]. Therefore, this study aimed to investigate the expression landscape

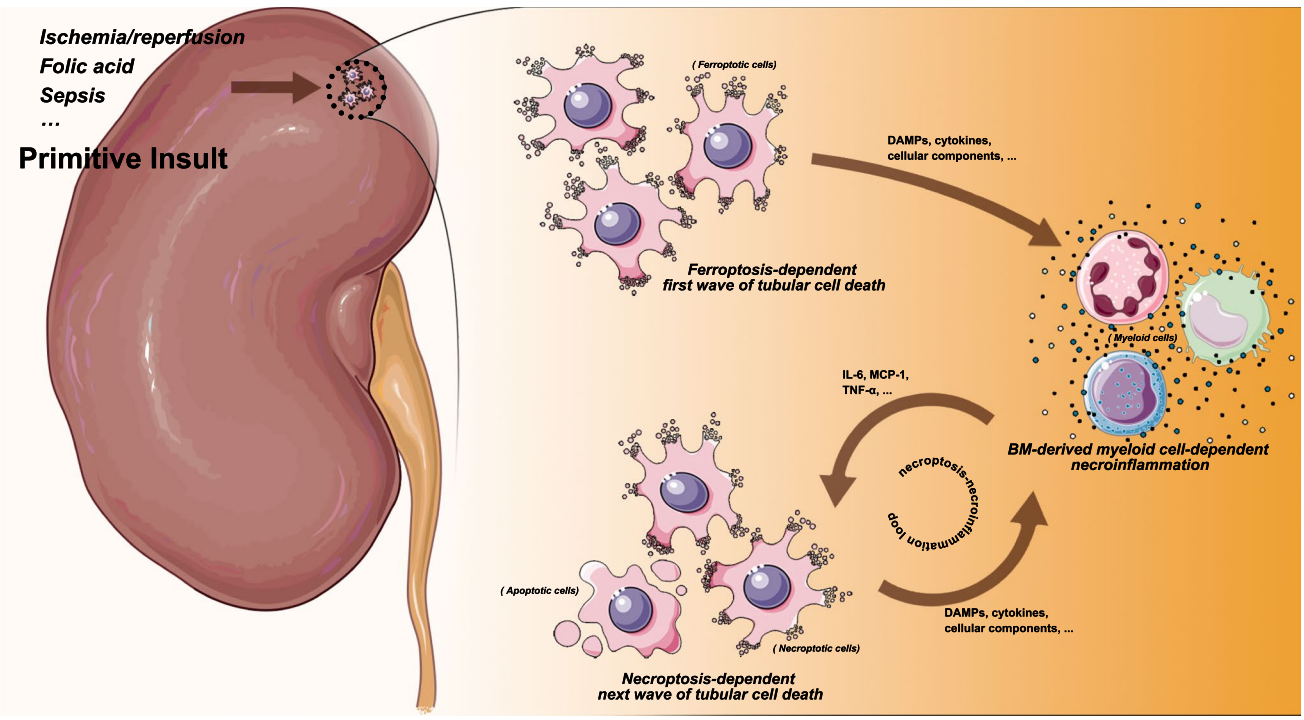

Fig. 1 Association between necroinflammation and tubular cell death. The primitive insult (ischemia/reperfusion, folic acid, sepsis, etc.) mediates the first wave of cell death and the release of DAMPs, cytokines, and cellular contents, thus inducing a loop between necroinflammation and the secondary wave of cell death. DAMPs, damage-associated molecular patterns; IL-6, interleukin-6; MCP-1, monocyte chemoattractant protein-1; TNF-α, tumor necrosis factor-α. Parts of the figure were drawn by using or modifying pictures from Servier Medical Art, provided by Servier, licensed under a Creative Commons Attribution 3.0 Unported License

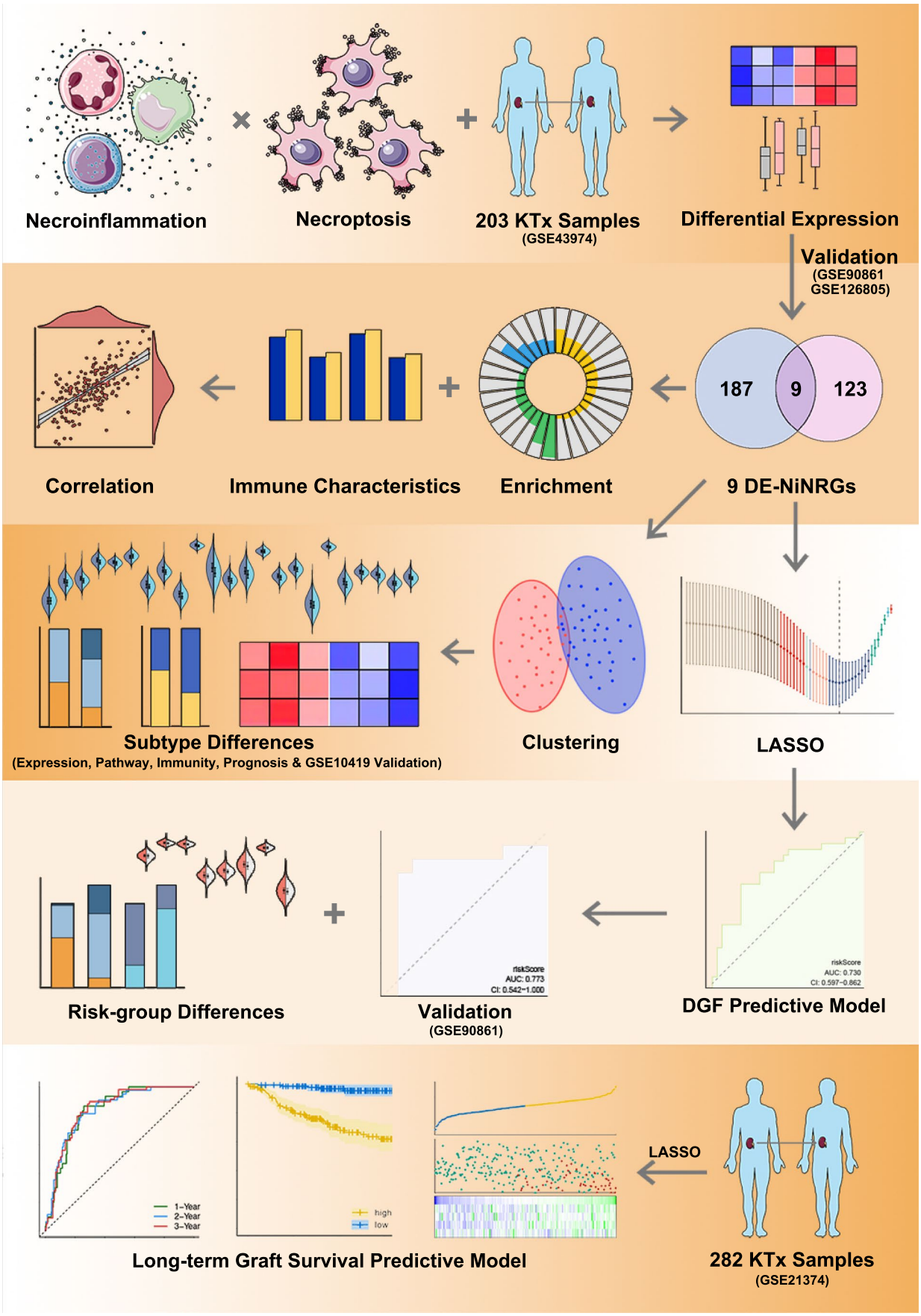
Necroinflammation
Necroptosis
203 KTx Samples
(GSE43974)
Differential Expression
Validation
(GSE90861
GSE126805)
187
9
123
9 DE-NiNRGs
Enrichment
Immune Characteristics
Correlation
LASSO
Clustering
Subtype Differences
(Expression, Pathway, Immunity, Prognosis & GSE10419 Validation)
DGF Predictive Model
riskScore
AUC: 0.730
CI: 0.597−0.862
Validation
(GSE90861)
riskScore
AUC: 0.773
CI: 0.542−1.000
Risk-group Differences
282 KTx Samples
(GSE21374)
LASSO
1−Year
2−Year
3−Year
high
low
Long-term Graft Survival Predictive Model

◂**Fig. 2** Flowchart of this study. DE-NiNRGs, differentially expressed necroinflammation-associated necroptosis-related genes; GF, graft function; KTx, kidney transplantation; LASSO, least absolute shrinkage and selection operator. Parts of the figure were drawn by using or modifying pictures from Servier Medical Art, provided by Servier, licensed under a Creative Commons Attribution 3.0 Unported License

of NiNRGs at the early stages after IRI, identify biomarkers, and construct predictive models of graft status by integrating machine learning algorithms based on the gene expression differences between test and control groups. In this work, we focused on the identification of KTx prognostic biomarkers by NiNRG expression profiling to provide a predictive tool for predicting DGF and graft loss, as well as a basis for individualized prevention and intervention to reach the goal of PPPM of improving graft survival and reducing the incidence of complications.

Study design

We downloaded the IRI-AKI-related datasets from the Gene Expression Omnibus (GEO) database and extracted the necroinflammation-related genes (NiRGs) and NRGs from the GeneCards website as well as previous reports. Subsequently, NiNRGs were obtained through a correlation analysis of NiRGs and NRGs, and the differentially expressed NiNRGs (DE-NiNRGs) were finally acquired based on the differentially expressed genes (DEGs) of the IRI-AKI dataset. These DE-NiNRGs were used to perform further analyses, such as the biological function annotation. We utilized DE-NiNRGs to conduct an unsupervised clustering of IRI samples to generate different necroinflammation-related necroptosis phenotypes, and a diagnostic model was constructed to predict the occurrence of post-IRI DGF and long-term graft loss by integrating machine learning. Furthermore, we analyzed the differences in gene expression, immune characteristics (including immune infiltration and immune response), and graft function among the different phenotypes and different prognostic risk groups. Figure 2 illustrates the step-by-step procedures of our study.

Materials and methods

Dataset acquisition and processing

Expression profiling by array or high-throughput sequencing was set as the prerequisite to retrieve KTx-, IRI-, DGF-, and allograft survival-related datasets from the GEO database (https://www.ncbi.nlm.nih.gov/geo/) [41]. Five datasets (summarized in Table S1) were finally chosen for the subsequent analysis and validation: (a) the GSE43974 dataset [42] consists of 188 pre-recover and 203 post-ischemia/reperfusion (IR) renal biopsies; (b) the GSE90861 dataset [43] contains 23 pairs of pre- and post-reperfusion biopsies, which 11 have been diagnosed as immediate graft function (IGF) and the other 12 as DGF; (c) the GSE126805 dataset [44] includes 41 and 42 kidney biopsies from before and after reperfusion, respectively; (d) the GSE10419 dataset [45] comprises 29 early post-KTx biopsies from 15 living and 14 DCD donors; and (e) the GSE21374 dataset [46] holds 282 late post-KTx biopsies. The R (version 4.1.2) packages "lumi" and "limma," as well as log2 transformation, were used for data normalization, transformation, background correction, and quality control.

Collection of NRGs and NiRGs

A total of 165 NRGs (Table S2) were acquired by running a search for "necroptosis" on GeneCrads (https://www.genecards.org/) with specific criteria (category protein coding and score > 0.8) or in previous reports [33–35, 47], and 88 NiRGs (Table S3) were obtained by running a search for "necroinflammation" with "protein coding" as the criterion on GeneCards.

DE-NiNRG identification and validation

The R package "limma" was employed to identify the positive DGEs in the GSE43974 dataset, with the cutoff criteria of a false detection rate (FDR) < 0.05 and a log2 fold change (logFC) > 0.5. The expression matrices of NiRGs and NRGs extracted from the GSE43974 dataset were correlated using the "cor.test" function of R software, and NiNRGs (Table S4) were output with the |correlation coefficient (R)| > 0.3 and a p value < 0.05. DE-NiNRGs were obtained by taking the intersection of DEGs and NiNRGs, which has been shown by the Venn network (Fig. 3B) drawn by EVenn [48]. The GSE90861 and GSE126805 datasets were set as two independent cohorts to further validate the post-IRI expression of DE-NiNRGs.

Exploration of the proteinaceous association of DE-NiNRGs

The protein–protein interaction (PPI) network demonstrates the known and potential associations among the proteins encoded by the nine DE-NiNRGs; this network was constructed by the STRING database [49] based on a certain criterion (organism: *Homo sapiens*; medium confidence: 0.400; FDR < 0.05).

Enrichment analysis of biological processes, molecular functions, and pathways

The Gene Ontology (GO) and Kyoto Encyclopedia of Genes and Genomes (KEGG) enrichment analyses of

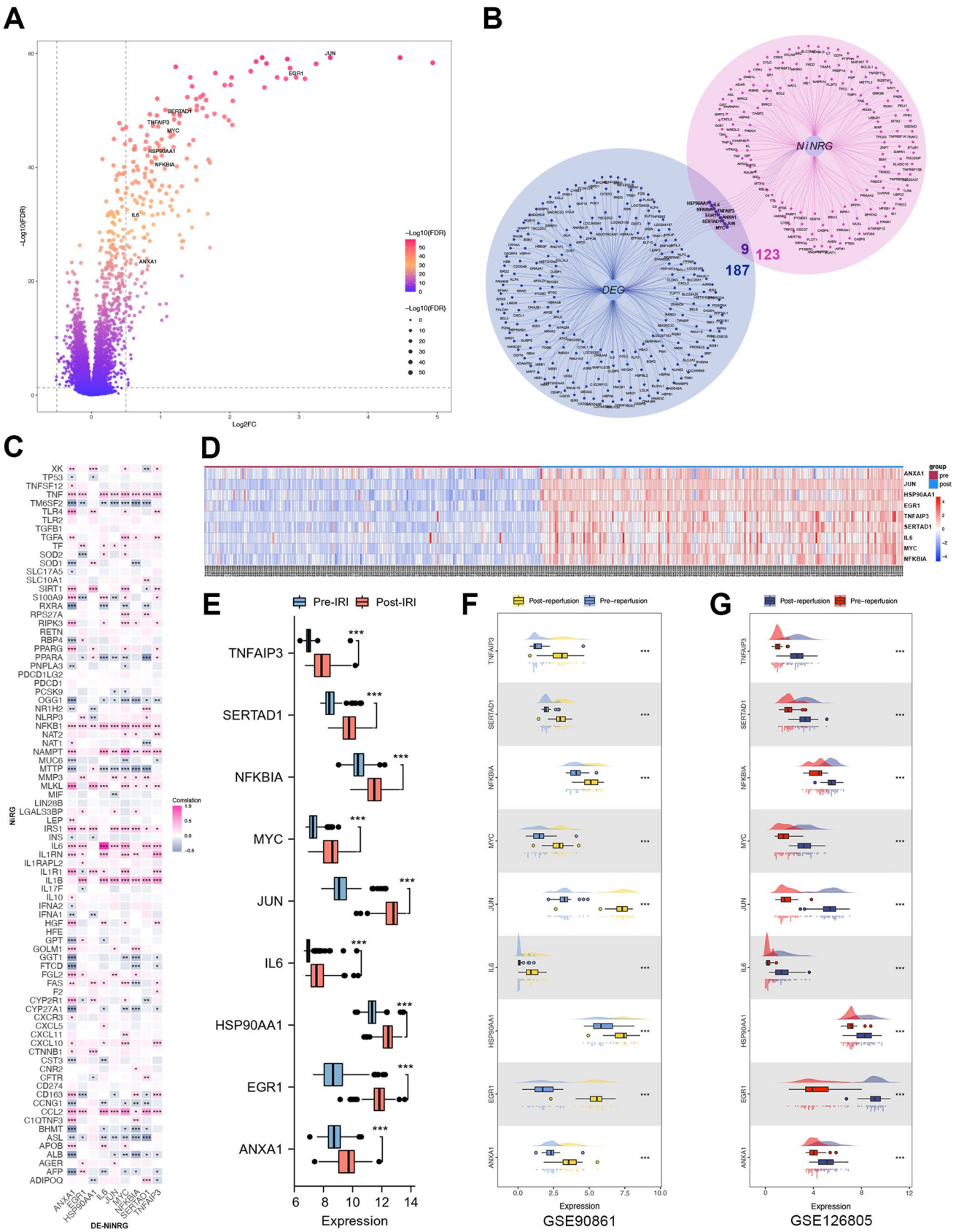
A
B
C
D
E
F
G
JUN
EGR1
SERTAD1
TNFAIP3
MYC
HSP90AA1
NFKBIA
IL6
ANXA1
−Log10(FDR)
Log2FC
NiNRG
DEG
9
123
187
DE-NiNRG
NiRG
Correlation
group
pre
post
Pre-IRI
Post-IRI
Expression
Post−reperfusion
Pre−reperfusion
GSE90861
GSE126805

◂**Fig. 3** Identification of the nine DE-NiNRGs in post-IRI KTx samples. **A** Volcano plot of DEGs with labeled DE-NiNRGs. **B** Venn network of the DEGs and NiNRGs. **C** Correlation of the NiRGs and nine DE-NiNRGs. **D** Expression heatmap of the nine DE-NiNRGs in control and post-IRI samples. **E** Box plot of the expression of the nine DE-NiNRGs at the two time points. **F**, **G** Raincloud plots showed the expression of the nine DE-NiNRGs in the validation datasets GSE90861 (**F**) and GSE126805 (**G**). DEG, differentially expressed gene; DE-NiNRG, differentially expressed NiNRG; IRI, ischemia/reperfusion injury; NiNRG, necroinflammation-associated NRG; NiRG, necroinflammation-related gene. *$p < 0.05$; **$p < 0.01$; ***$p < 0.001$

DE-NiNRGs were conducted using the R package "clusterProfiler" [50], with the two gene annotations obtained via the R package "org.Hs.eg.db" and the KEGG rest application programming interface (https://www.kegg.jp/kegg/rest/keggapi.html) [51] as the background (Tables S5 and S6). Gene set variation analysis (GSVA) was conducted using the R package "GSVA," referring to the H: hallmark gene sets (h.all.v2022.1.Hs.symbols.gmt) obtained from the Molecular Signatures Database (MSigDB; http://www.gsea-msigdb.org/gsea/msigdb/index.jsp) [52], to identify the biological pathway differences in two IRI subtypes (Table S7). The significantly enriched functions and pathways were output when the FDR was < 0.05.

Analysis of immune characteristics

To understand the immune characteristics, single sample gene set enrichment analysis (ssGSEA) was applied to estimate the abundance of immune cell populations and the activity of immune response in each sample via the following R packages: "GSVA" and "GSEABase." The abundance of macrophages and neutrophils was further validated by TIMER [53], xCELL [54], and ImmuCellAI [55]. The R function "cor.test" contributed to the correlation analysis of immune characteristics and DE-NiNRGs.

Consensus clustering

To determine distinct necroinflammation-related necroptosis subtypes, a cluster analysis of all the IRI samples in the GSE43974 dataset was performed using the R package "ConsensusClusterPlus" [56] based on the expression of DE-NiNRGs; the number of clusters (k) was set between 2 and 8; the "partitioning around medoids" cluster algorithm with "1-Spearman correlation" distance was used; and 80% of the samples were resampled for 50 repetitions. The determination of the optimal k was dependent on the best consensus among the items in each cluster.

Machine learning-based construction of the post-KTx DGF predictive model

First, 202 post-IRI early KTx samples from the GSE43974 dataset recorded with graft function were divided 7:3 into training and internal testing sets using the R package "caret." Subsequently, the candidate genes with their regression coefficients were further generated from the training set by the tenfold cross-validated least absolute shrinkage and selection operator (LASSO) [57] regression using the R package "glmnet." Binominal deviance values were used to select the key λ values by using the minimum criteria (lambda.min) and the 1 standard error of the minimum criteria (lambda.1se). Variables with non-zero coefficients decrease with increasing λ. Based on the minimum criterion, lambda.min was identified as the optimal λ. The candidate genes and coefficients can be identified by the optimal λ, and then the model is constructed. Furthermore, the risk scores were calculated using a linear combination of the regression coefficient and the expression of candidate genes ($\text{Riskscore} = \sum_{i=1}^{n}[\text{geneCoef}_i \times \text{geneExp}_i]$). The model's robustness was validated by the internal testing set and an external set (the GSE90861 dataset), and the performance was evaluated through the receiver operating characteristic (ROC) curves based on the risk scores. Moreover, in agreement with the ratio of the sample sizes of DGF and IGF, risk scores were used to organize the IRI patients into high- and low-risk groups for the subsequent study.

Recognition of long-term allograft survival-related DE-NiNRGs

Considering the potentially vicious cycle of necroinflammation and necroptosis, we explored the impact of the sustained expression of these genes on long-term graft survival. Univariable Cox regression (hazard ratio (HR) ≠ 1 and p value < 0.05) was used to screen out long-term prognosis-related DE-NiNRGs using the R package "survival," referring to the GSE21374 dataset.

Construction of the graft survival predictive model

For the long-term prognosis-related DE-NiNRGs expression matrix extracted from the GSE21374 dataset (all samples were divided 7:3 randomly into training and testing groups), the predictive genes and coefficients were established through the LASSO regression algorithm with tenfold cross-validation; the time-dependent ROC curves were used to illustrate the performance of the model. Based on the risk scores ($\text{Riskscore} = \sum_{i=1}^{n}[\text{geneCoef}_i \times \text{geneExp}_i]$) and their median, the 206 samples with graft status information within 3 years (105 graft survival and 51 graft loss samples; 56 rejection and 150 non-rejection samples) from the

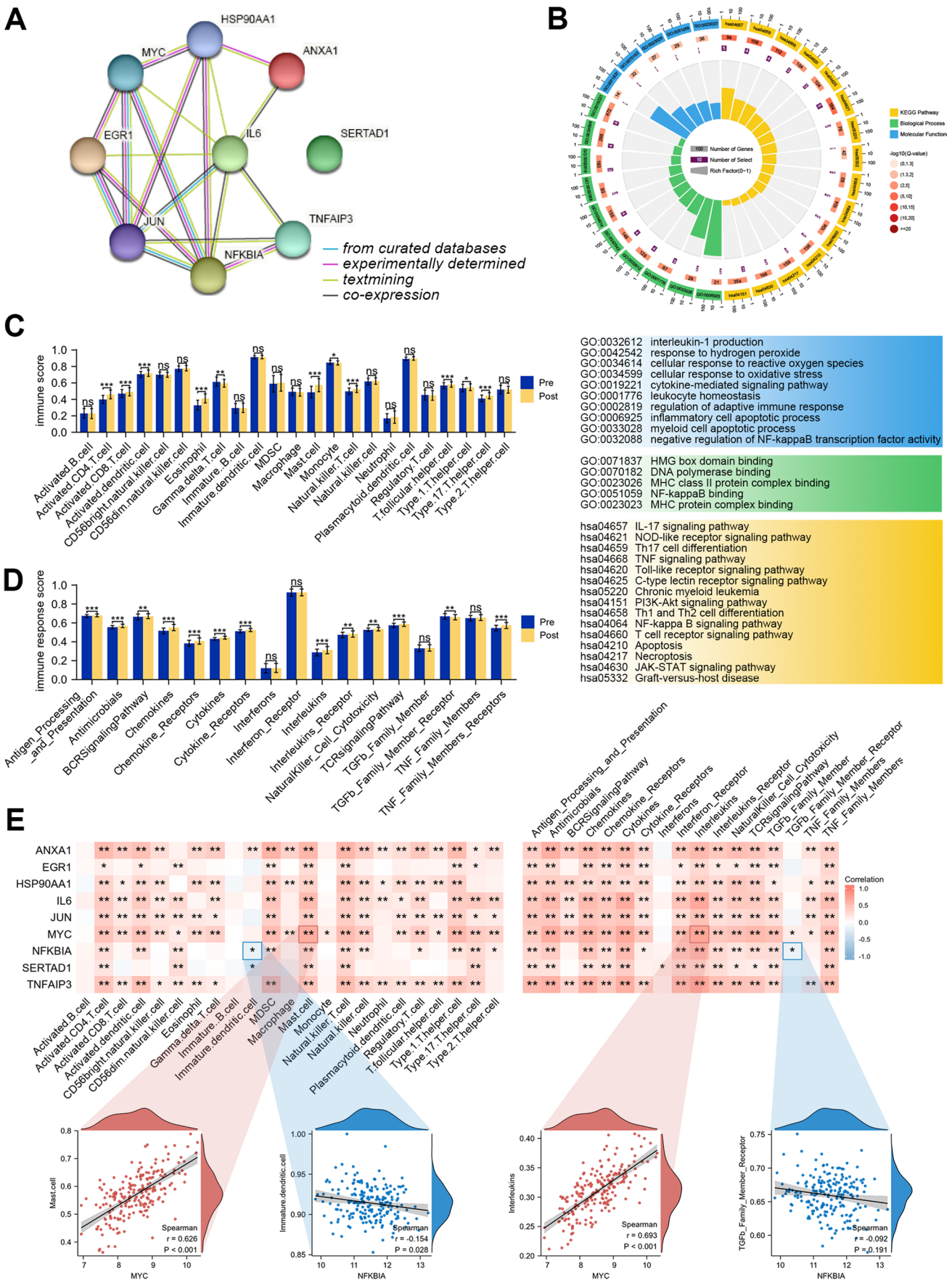
A
HSP90AA1
MYC
ANXA1
EGR1
IL6
SERTAD1
JUN
TNFAIP3
NFKBIA
from curated databases
experimentally determined
textmining
co-expression
B
KEGG Pathway
Biological Process
Molecular Function
-log10(Q-value)
Number of Genes
Number of Select
Rich Factor(0~1)
C
immune score
Pre
Post
Activated.B.cell
Activated.CD4.T.cell
Activated.CD8.T.cell
Activated.dendritic.cell
CD56bright.natural.killer.cell
CD56dim.natural.killer.cell
Eosinophil
Gamma.delta.T.cell
Immature..B.cell
Immature.dendritic.cell
MDSC
Macrophage
Mast.cell
Monocyte
Natural.killer.T.cell
Natural.killer.cell
Neutrophil
Plasmacytoid.dendritic.cell
Regulatory.T.cell
T.follicular.helper.cell
Type.1.T.helper.cell
Type.17.T.helper.cell
Type.2.T.helper.cell
GO:0032612 interleukin-1 production
GO:0042542 response to hydrogen peroxide
GO:0034614 cellular response to reactive oxygen species
GO:0034599 cellular response to oxidative stress
GO:0019221 cytokine-mediated signaling pathway
GO:0001776 leukocyte homeostasis
GO:0002819 regulation of adaptive immune response
GO:0006925 inflammatory cell apoptotic process
GO:0033028 myeloid cell apoptotic process
GO:0032088 negative regulation of NF-kappaB transcription factor activity
GO:0071837 HMG box domain binding
GO:0070182 DNA polymerase binding
GO:0023026 MHC class II protein complex binding
GO:0051059 NF-kappaB binding
GO:0023023 MHC protein complex binding
hsa04657 IL-17 signaling pathway
hsa04621 NOD-like receptor signaling pathway
hsa04659 Th17 cell differentiation
hsa04668 TNF signaling pathway
hsa04620 Toll-like receptor signaling pathway
hsa04625 C-type lectin receptor signaling pathway
hsa05220 Chronic myeloid leukemia
hsa04151 PI3K-Akt signaling pathway
hsa04658 Th1 and Th2 cell differentiation
hsa04064 NF-kappa B signaling pathway
hsa04660 T cell receptor signaling pathway
hsa04210 Apoptosis
hsa04217 Necroptosis
hsa04630 JAK-STAT signaling pathway
hsa05332 Graft-versus-host disease
D
immune response score
Pre
Post
Antigen_Processing_and_Presentation
Antimicrobials
BCRSignalingPathway
Chemokines
Chemokine_Receptors
Cytokines
Cytokine_Receptors
Interferons
Interferon_Receptor
Interleukins
Interleukins_Receptor
NaturalKiller_Cell_Cytotoxicity
TCRsignalingPathway
TGFb_Family_Member
TGFb_Family_Member_Receptor
TNF_Family_Members
TNF_Family_Members_Receptors
E
ANXA1
EGR1
HSP90AA1
IL6
JUN
MYC
NFKBIA
SERTAD1
TNFAIP3
Correlation
Mast.cell
MYC
Spearman
r = 0.626
P < 0.001
Immature.dendritic.cell
NFKBIA
Spearman
r = -0.154
P = 0.028
Interleukins
MYC
Spearman
r = 0.693
P < 0.001
TGFb_Family_Member_Receptor
NFKBIA
Spearman
r = -0.092
P = 0.191

◂**Fig. 4** Interaction, functional enrichment, and immune characteristic analysis of the DE-NiNRGs. **A** Protein–protein interactions among the nine DE-NiNRGs. **B** Biological process, molecular function, and KEGG pathway annotation of the nine DE-NiNRGs. **C**, **D** Differences in immune infiltration (**C**) and immune response activity (**D**) before and after IRI. **E** Correlation between the DE-NiNRGs and immune characteristics. MDSC, myeloid-derived suppressor cell. $^{*}p < 0.05$; $^{**}p < 0.01$; $^{***}p < 0.001$; ns, $p \geq 0.05$

GSE21374 were subsequently divided into two different risk groups of graft loss. The prognostic differences between the two groups were assessed using the Kaplan–Meier (K–M) graft survival analysis, risk curve, and Chi-square test.

Statistical analysis

R software was utilized to carry out the statistical analysis. The distributions of continuous and nominal variables were characterized by descriptive statistics. Student's *t*-test and Mann–Whitney *U* nonparametric test were applied to normal and abnormal distribution variables, respectively. The differences between the two IRI subtypes and risk groups of classified data were appraised using a two-sided Chi-square test, and Fisher's exact test was used instead when the total sample size was less than 40. Pearson's correlation method was employed to identify the association between genes and immune characteristics; a *p* value or DFR < 0.05 indicated statistical significance, while $|R| > 0.3$ was considered to be correlated.

Results

The early expression landscape of necroinflammation-correlated NRGs in the KTx patients

A differential expression analysis of the expression profiles from 188 pre-IR and 203 post-IR kidney biopsies (underwent cold ischemia and were recovered 1 h after reperfusion) yielded a total of 196 upregulated DEGs (Fig. 3A). Furthermore, as described in previous sections, considering the close association between necroinflammation and necroptosis, 132 NiNRGs were obtained via a correlation analysis of the extracted expression matrices of the NiRGs and NRGs (Fig. S1; Table S4). Based on the DEGs and NiNRGs, nine genes (*ANXA1*, *EGR1*, *HSP90AA1*, *IL6*, *JUN*, *MYC*, *NFKBIA*, *SERTAD1*, and *TNFAIP3*) were finally identified as DE-NiNRGs; these are shown by the Venn network (Fig. 3B) and positioned in the volcano diagram (Fig. 3A). Notably, in accordance with the current understanding, these genes exhibited a more positive correlation with necroinflammation according to our analysis (Fig. 3C). The heat map and box plot more clearly present the expression landscape of the nine DE-NiNRGs in the control and IR kidney biopsies (Fig. 3D–E). To exclude any interference resulting from chance, we also validated the expression of the nine DE-NiNRGs in two additional independent KTx profiles; the consistent results further demonstrated the upregulation and significance of these genes in the IR kidneys (Fig. 3F, G).

Interactions, functions, and immune correlation of DE-NiNRGs

To capture the potential associations and bio-functions involved in the nine DE-NiNRGs, these genes were subjected to functional enrichment analysis. As shown by the PPI network, the proteins encoded by DE-NiNRGs, with the exception of SERTAD1, are considered to engage in a high degree of interaction (Fig. 4A). Further results showed that these genes are involved in signaling pathways such as necroptosis, apoptosis, graft-versus-host disease, and inflammatory and immune responses, based on the KEGG pathway analysis; this is generally consistent with the annotation results of biological and molecular functions (Fig. 4B; Tables S5 and S6). Therefore, we analyzed the differences in the abundance of immuno-infiltration and activity of the immune response at the early stage of IR compared to controls. While the immune infiltration analysis did not show many differences, there was a broad upregulation of pathways related to inflammation and the immune response early after IR (Fig. 4C, D); it should be noted that these results were also influenced by potential graft rejection. The correlation heat map further shows the potential relationships between the nine DE-NiNRGs and these immune characteristics (Fig. 4E). In particular, we extracted and exhibited the most positive and most negative associations: *MYC* was most positively correlated with mast cells and interleukins, whereas *NFKBIA* was most negatively correlated with immature dendritic cells (DCs) and the TGFb family member receptor (Fig. 4E).

Identification of necroinflammation-correlated necroptosis subtypes in the IRI patients

The degree of IRI varies from patient to patient, resulting in different extents of tubular cell death and thus causing different graft functions. Therefore, we aimed to investigate the differences between the subtypes by stratifying 203 IRI patients on the basis of the expression of the nine DE-NiNRGs. We prioritized the consensus of items within the clusters to obtain the best *k* based on the consensus clustering results (Fig. 5B). Ultimately, compared to the other values for *k* (Fig. S2), the IRI samples could be divided into two subtypes (Fig. 5A): cluster A ($n = 92$) and cluster B ($n = 111$). The principal component analysis (PCA) indicated a remarkable difference in DE-NiNRG expression between

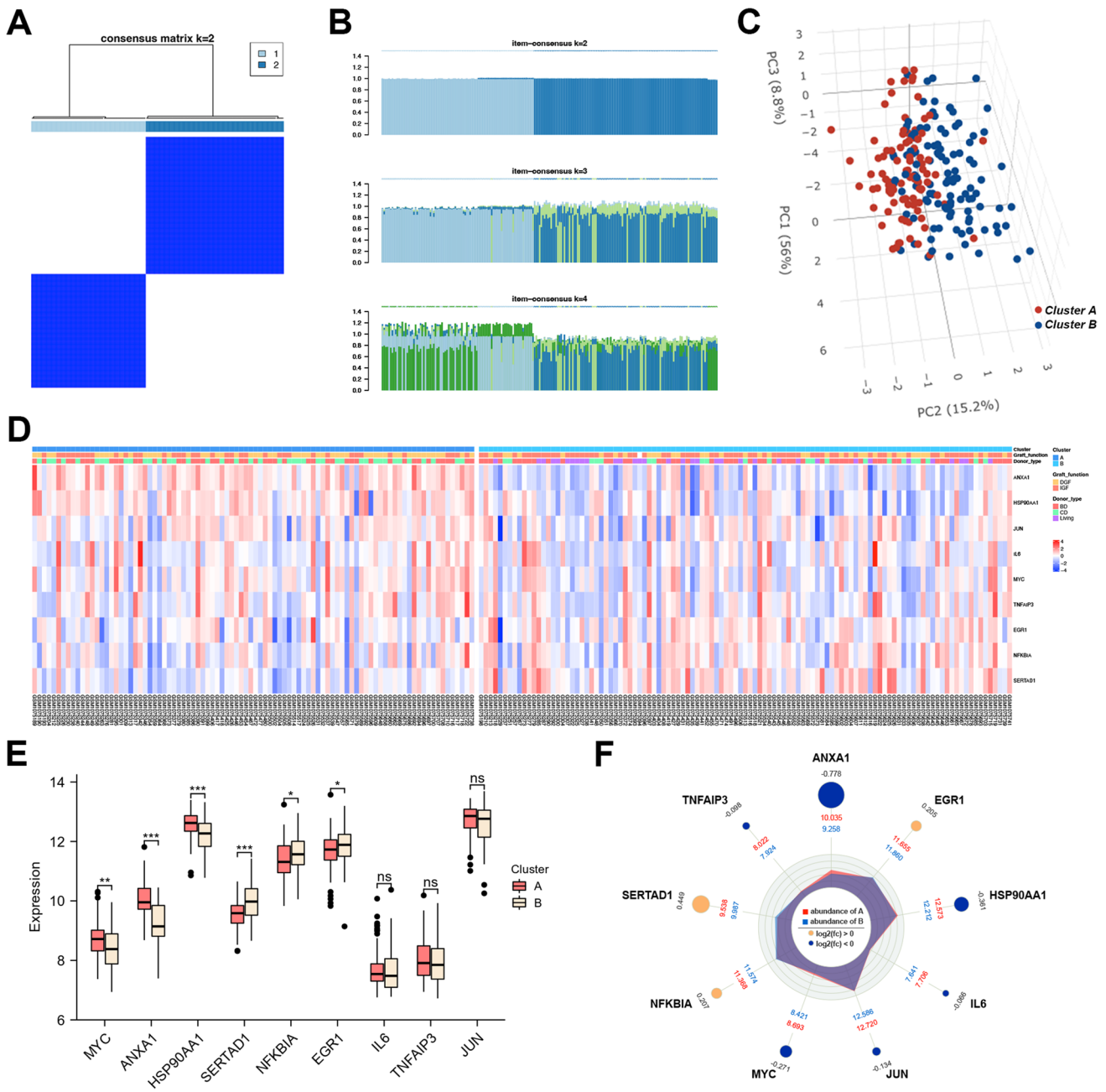

Fig. 5 Identification of two IRI subtypes based on the DE-NiNRGs. **A** Consensus clustering matrix for $k=2$. **B** Consensus of the items ($k=2$–4) in each cluster. **C** Three-position PCA plot showing expression patterns of DE-NiNRGs between the two clusters. **D–F** Expression differences of the nine DE-NiNRGs between the two subtype clusters shown in the heatmap (**D**), box plot (**E**), and radar plot (**F**). BD, brain dead; CD, cardiac dead; DGF, delayed graft function; IGF, immediate graft function. $^{*}p<0.05$; $^{**}p<0.01$; $^{***}p<0.001$; ns, $p\geq0.05$

the two IRI subtypes (Fig. 5C). Gene expression differences were observed using a heat map (Fig. 5D). In particular, compared to cluster A, cluster B exhibited a higher expression of *ANXA1*, *HSP90AA1*, and *MYC*, while *EGR1*, *NFKBIA*, and *SERTAD1* were downregulated; the remaining three DE-NiNRGs (*IL6*, *JUN*, and *TNFAIP3*) were not differentially expressed (Fig. 5E, F). The differential expression of the DE-NiNRGs suggests potential differences in the extent of necroptosis in the two subtypes. The increasing levels of ANXA1 and HSP90AA1, as two DAMPs (key components in the necroinflammation-associated necroptosis loop; Fig. 1) [37], may predict more severe cell death. However, the upregulation of NFKBIA—a classical inhibitor of the NF-κB pathway (another important pathway involved in

the necroinflammation-induced necroptosis process) [12, 38]—appears to limit cell loss. These results suggested that cluster B patients may experience milder necroptosis and necroinflammation and were thus associated with distinct clinical features (Fig. 5D).

Immune characteristics, enrichment features, and clinical correlation of the two IRI subtypes

We explored the differences between the biological characteristics of the two IRI clusters. The immune signature analysis revealed a distinct difference in immune activity between the two clusters. Compared to Cluster A, Cluster B exhibited an extensive downregulation of immune infiltration, accompanied by a lower activity of the immune response (Fig. 6A); this is in line with our previous discussion. To further explore whether the expression of bio-pathways differed between the two IRI clusters, we performed a GSVA enrichment analysis based on the H: hallmark gene sets obtained from MSigDB (Table S7). The heat map shows the top 15 differentially expressed pathways based on FDRs (Fig. 6B). Notably, all 15 pathways were activated less in cluster B, especially allograft rejection, inflammation response, INF-α/γ response, IL6-JAK-STAT3 signaling, and IL2-STAT5 signaling (Fig. 6C, D).

Following this, the clinical features of the two subtypes were next revealed. In accordance with our findings, compared to Cluster A, the quantity and proportion of DGF in cluster B were noticeably lower ($p = 0.001$), which seemed to indicate a better short-term prognosis (Fig. 6F). Regarding the types of donors, there are three kinds: living, DCD, and DBD donors. While there were no differences associated with DBD donors between the two groups, the other two types showed contrasting results ($p < 0.0001$): living donors were completely classified into the cluster B subtype, while cluster A had a higher proportion of DCD donors (Fig. 6E). We attempted to explore the expression differences in post-KTx biopsies from different donors based on a new dataset (GSE10419) for the purpose of validation. Compared to living donor kidneys, kidneys extracted from DCD donors appeared to have an upregulation of *ANXA1*, *HSP90AA1*, and *MYC* after IR, which is in line with the results for cluster A (Fig. 6G).

Construction and validation of a DGF predictive model based on DE-NiNRGs

The three candidate genes (*ANXA1*, *HSP90AA1*, and *NFKBIA*), with their regression coefficients (Fig. 7A–C; Table S8), used to construct the DGF predictive model, were selected from the training set (constructed by randomly selecting 70% of the 202 IRI samples from the GSE43974 dataset) via the LASSO regression algorithm derived from the expression of the nine DE-NiNRGs. The accuracy of the risk score for the model was assessed using the ROC curve, and the area under the curve (AUC) was 0.791, 0.730, and 0.772 for the training set, the internal testing set, and the complete set, respectively (Fig. 7D–F). Furthermore, the GSE90861 dataset was used for further validation as an external test set, and the AUC was 0.773 (Fig. 7G).

Clinical characteristics and myeloid immune infiltration of the different DGF risk groups

The IRI sample was grouped by the risk scores. The high-risk group retained higher amounts of DGF ($p < 0.0001$, Fig. 7H), which was also obtained in the external validation set ($p = 0.0033$, Fig. 7I). The donation of kidneys is closely linked to the occurrence of DGF; in particular, patients who receive kidneys from DCD donors experience a greater proportion of DGF [58, 59]. The subsequent analysis also demonstrated differences in kidney donation between the two groups. The high-risk group had more DCD donors, while the low-risk group had more living and DBD donors ($p < 0.0001$, Fig. 8A). Notably, the test of the variances in the subtype composition of the two risk groups showed that cluster B was more associated with lower risk ($p < 0.0001$), confirming our previous suppositions (Fig. 8A). The Sankey diagram visualizes the composition of donor type, graft function, subtype, and DGF risk in IRI samples (Fig. 8B).

Recent reports have suggested that myeloid immune cells may be critical for necroinflammation-mediated next wave of cell death, especially macrophages, DCs, and neutrophils [34, 35]. Therefore, we assessed the myeloid immune cell infiltration difference of the two risk groups using ssGSEA, which revealed a higher abundance of immature or plasmacytoid DCs, eosinophils, and macrophages in the high-risk group (Fig. 8C). Afterward, the abundance of both macrophages and neutrophils was further evaluated using three other algorithms: TIMER, xCELL, and ImmuCellAI. In contrast to ssGSEA, these three algorithms showed differences in neutrophils between the two groups. Furthermore, the xCELL-based results demonstrated that macrophage differences seem to arise mainly from the M1 type rather than the M2 type (Fig. 8C).

Exploration of NiNRGs for predicting long-term graft survival

A continuous loop between necroinflammation and programmed necrosis is conceivable in the absence of effective intervention. We noticed that the graft rejection pathway was more activated in cluster A (Fig. 6B–D). As the occurrence of post-KTx DGF often leads to chronic rejection and future allograft loss, we further explored the potential of DE-NiNRGs for predicting graft survival time after a biopsy. The

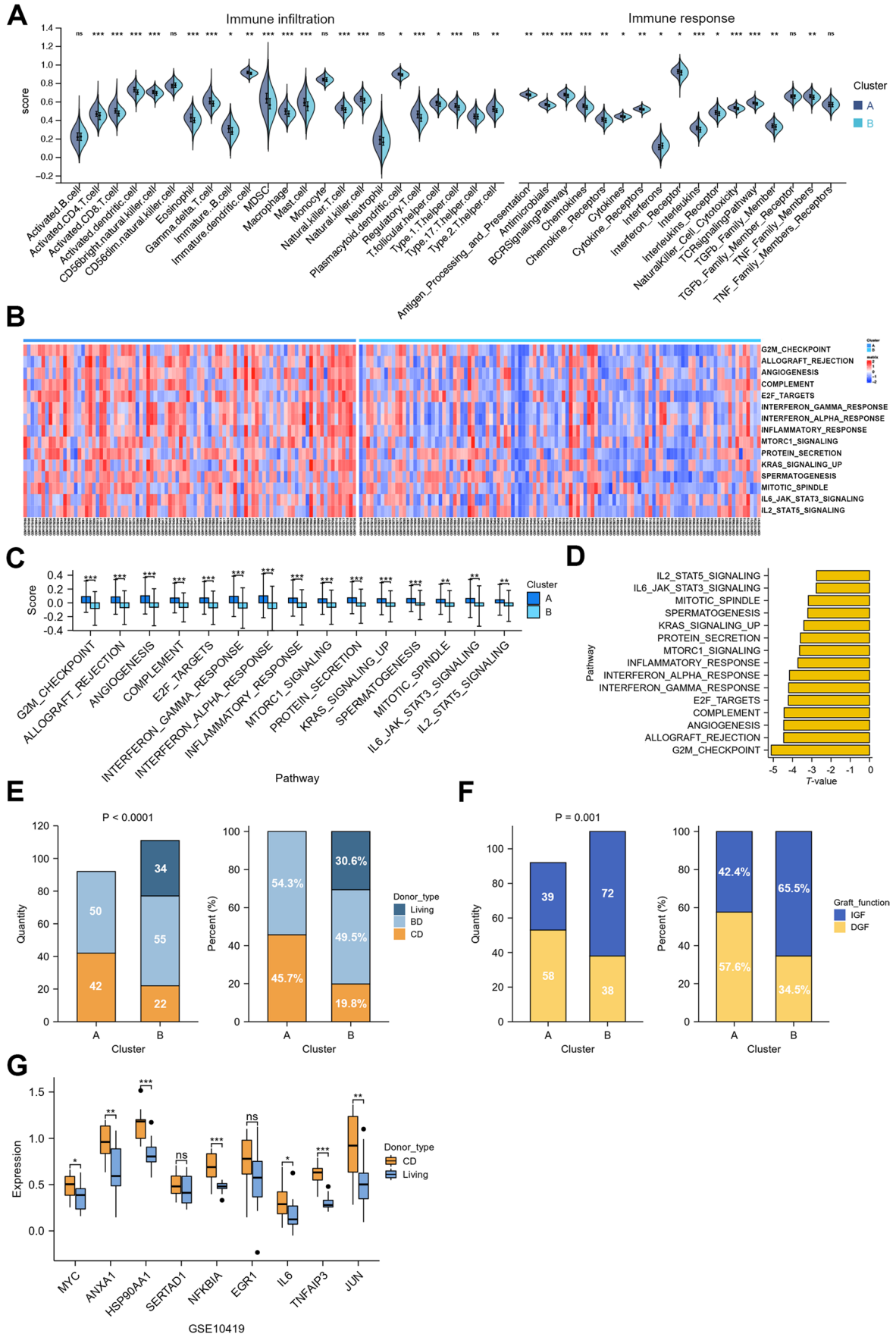
A
Immune infiltration
Immune response
score
Cluster
A
B
Activated.B.cell
Activated.CD4.T.cell
Activated.CD8.T.cell
Activated.dendritic.cell
CD56bright.natural.killer.cell
CD56dim.natural.killer.cell
Eosinophil
Gamma.delta.T.cell
Immature.B.cell
Immature.dendritic.cell
MDSC
Macrophage
Mast.cell
Monocyte
Natural.killer.T.cell
Natural.killer.cell
Neutrophil
Plasmacytoid.dendritic.cell
Regulatory.T.cell
T.follicular.helper.cell
Type.1.T.helper.cell
Type.17.T.helper.cell
Type.2.T.helper.cell
Antigen_Processing_and_Presentation
Antimicrobials
BCRSignalingPathway
Chemokine_Receptors
Chemokines
Cytokine_Receptors
Cytokines
Interferon_Receptor
Interferons
Interleukin_Receptor
Interleukins
Interleukins_Receptor
NaturalKiller_Cell_Cytotoxicity
TCRsignalingPathway
TGFb_Family_Member
TGFb_Family_Member_Receptor
TNF_Family_Members
TNF_Family_Members_Receptors
B
G2M_CHECKPOINT
ALLOGRAFT_REJECTION
ANGIOGENESIS
COMPLEMENT
E2F_TARGETS
INTERFERON_GAMMA_RESPONSE
INTERFERON_ALPHA_RESPONSE
INFLAMMATORY_RESPONSE
MTORC1_SIGNALING
PROTEIN_SECRETION
KRAS_SIGNALING_UP
SPERMATOGENESIS
MITOTIC_SPINDLE
IL6_JAK_STAT3_SIGNALING
IL2_STAT5_SIGNALING
C
Score
Cluster
A
B
Pathway
D
Pathway
T-value
E
P < 0.0001
Quantity
Percent (%)
Donor_type
Living
BD
CD
Cluster
F
P = 0.001
Graft_function
IGF
DGF
G
Expression
Donor_type
CD
Living
MYC
ANXA1
HSP90AA1
SERTAD1
NFKBIA
EGR1
IL6
TNFAIP3
JUN
GSE10419

◂**Fig. 6** Immune characteristics, biological pathways, and clinical correlations of the two subtypes. **A** Inter-subtype differences in immune infiltration and immune response activity. **B**, **C** Heatmap (**B**) and box plot (**C**) showed the different hallmarks between the two clusters. **D** *T* value of the GSVA analysis. **E**, **F** Stacked bar charts compare the differences in donor type (**E**) and graft function (**F**) between the two clusters. **G** Comparison of DE-NiNRG expression between CD and living donors in dataset GSE10419. CD, cardiac dead; DGF, delayed graft function; IGF, immediate graft function. *$p < 0.05$; **$p < 0.01$; ***$p < 0.001$; ns, $p \geq 0.05$

long-term prognosis-related DE-NiNRGs (*ANXA1*, *NFKBIA*, *IL6*, *JUN*, *EGR1*, *MYC*, and *TNFAIP3*) in the GSE21374 dataset that were screened using univariate Cox regression are displayed in the forest plot (Fig. 9A).

We randomized all of the recipients in the GSE21374 dataset into two sets (in a 7:3 division) for training and testing, respectively. Based on the seven prognostic NiNRGs, the LASSO regression analysis was conducted for the training set to identify the risk genes, and five genes were finally selected (*ANXA1*, *EGR1*, *JUN*, *MYC*, and *NFKBIA*; Fig. 9B–C). The final risk score for each sample was obtained by summing the products of gene expression and coefficients (Fig. 9D; Table S9). In the training set, the time-dependent ROC curves yielded the AUCs (0.817, 0.852, and 0.862) of risk scores for 1–3 years of survival; the corresponding values in the test set were 0.770, 0.702, and 0.735, respectively (Fig. 9E, F). The predictive accuracy of the risk score in the complete set was 0.802, 0.814, and 0.833 (Fig. 9G). These results demonstrated that the seven-NiNRG predictive model was capable of predicting the long-term prognosis of allografts.

By grouping patients (based on the median risk scores), we compared the differences in graft loss and rejection between the two risk groups. Obviously, the higher-risk recipients were more likely to suffer allograft loss (Fig. 10A, B). Similar results are also reflected in graft rejection (Fig. 10C). The K–M curve intuitively shows that outcomes became worse in the high-risk group as the year increased (Fig. 10D). Finally, we summarized the composition of the patients using the Sankey diagram (Fig. 10E).

Discussion

In this study, we first comprehensively explored the necroinflammation-associated necroptosis in the early post-IRI stage and its impact on short-term graft function and long-term graft survival. NiNRGs were obtained using correlation analysis, and we selected nine upregulated DE-NiNRGs (*ANXA1*, *EGR*, *HSP90AA1*, *IL6*, *JUN*, *MYC*, *NFKBIA*, *SERTAD1*, and *TNFAIP3*) in the post-IR renal biopsies. Based on the expression profile of DE-NiNRGs, we clustered the post-KTx IRI patients to determine the biological processes, immune characteristics, and clinical features of the two different subtypes. Finally, we constructed a DE-NiNRG-dependent DGF and long-term graft survival prediction model with good predictive validity.

Current knowledge of cell death in IRI-AKI

The post-AKI cell death process has been attracting increasing attention from researchers. According to the latest consensus of the Nomenclature Committee on Cell Death in 2018, cell death can be classified into accidental cell death and RCD; the latter can be further divided into 12 forms, namely intrinsic apoptosis, extrinsic apoptosis, mitochondrial permeability transition-driven necrosis, necroptosis, ferroptosis, pyroptosis, parthanatos, entosis, NETosis, lysosome-dependent cell death, autophagy-dependent cell death, and immunogenic cell death [60]. In addition, some other types of cell death are being increasingly reported, including calcicoptosis [61] and cuproptosis [62]. Researchers have long sought to understand which cell deaths contribute to the loss of renal tubular cells, as well as the proportion, order, and crosstalk of these cell deaths. Pathologists initially described the histopathological changes after IRI-AKI as acute tubular necrosis (ATN), until it was first linked with apoptosis by Schumer et al. in 1992 [63]. Afterward, as the understanding deepened, more evidence for the involvement of cell death in AKI was presented, especially for ferroptosis [64] and necroptosis [65]. However, recently, there has been further understanding of such cell deaths during AKI, as detailed in the previous sections. Therefore, while blocking ferroptosis resulted in a greater benefit for renal hypofunction within the initial 24 h after reperfusion, the vehicle targeting the necroinflammatory-associated necroptosis-associated pathway did cut off the vicious loop to prevent the ensuing cell loss [32–34, 66]. Consequently, early mitigation of cell loss is crucial to achieving PPPM in post-KTx patients.

Expected impact of the current study on the PPPM model for maintaining graft adaptation

Achieving PPPM is an exciting vision for the field of transplantation medicine. As we have discussed previously, multi-stage prediction, prevention, and treatment should be applied to the management of post-KTx complications.

First stage

Identifying prognosis-related factors in the donor's kidney during the pre-transplant stage. For example, the available evidence suggests an association between donor-specific antibodies and poor KTx outcomes [7, 67]. Furthermore, exploring the impact of pre-donor and pre-transplant therapy

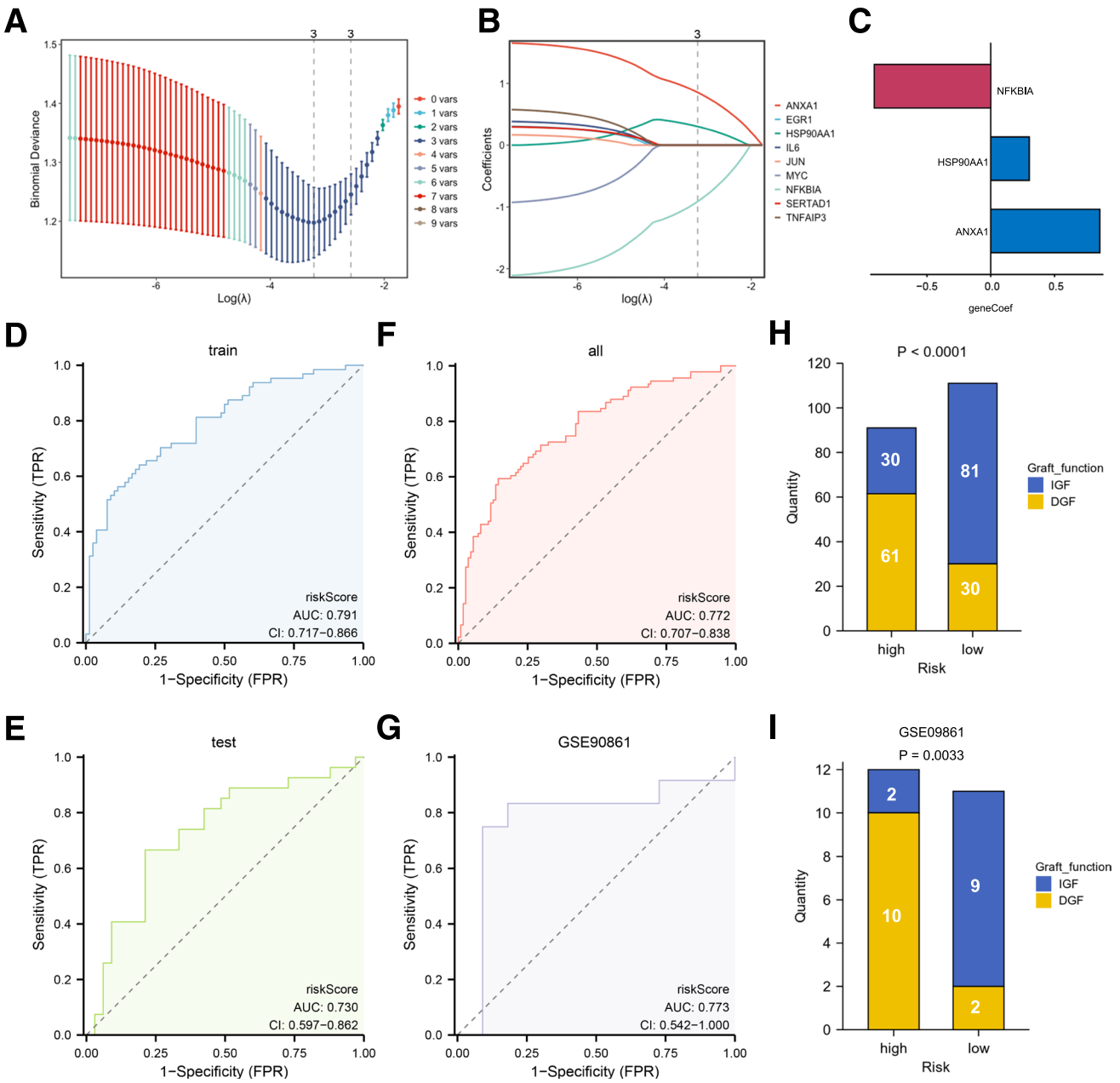

Fig. 7 Establishment and validation of the DGF predictive model. **A** Selecting λ in the LASSO model using tenfold cross-validation. Two vertical dotted lines were drawn at the lambda.min (the optimal λ, left) and lambda.1se (right). **B** LASSO coefficient profiles of the nine DE-NiNRGs. The dotted line was drawn at the optimal λ and resulted in 3 nonzero coefficients. **C** Coefficients of the candidate NiNRGs. **D**, **E** The ROC curves show the performance of the model on the training set (**D**), the internal test set (**E**), and the complete set (**F**). **G** Validation of the DGF predictive model on the external test set GSE90861 by ROC curves. **H**, **I** Donor type differences between the high- and low-risk groups of the whole set (**H**) and external test set (**I**). AUC, area under the curve; DGF, delayed graft function; IGF, immediate graft function

on the renal allograft. Ngamvichchukorn et al. revealed that pre-transplant peritoneal dialysis was associated with a lower risk of overall graft loss and DGF, but more data is needed to validate this finding [68]. Moreover, more accurate donor–recipient matching, shorter ischemic period, and more suitable graft storage conditions are also essential.

Second stage

Early post-KTx prediction of complications, especially DGF, is crucial for intervention, which is the objective of our work. DGF is strongly implicated in higher rates of allograft rejection and inferior short- or long-term prognosis [4, 69], which

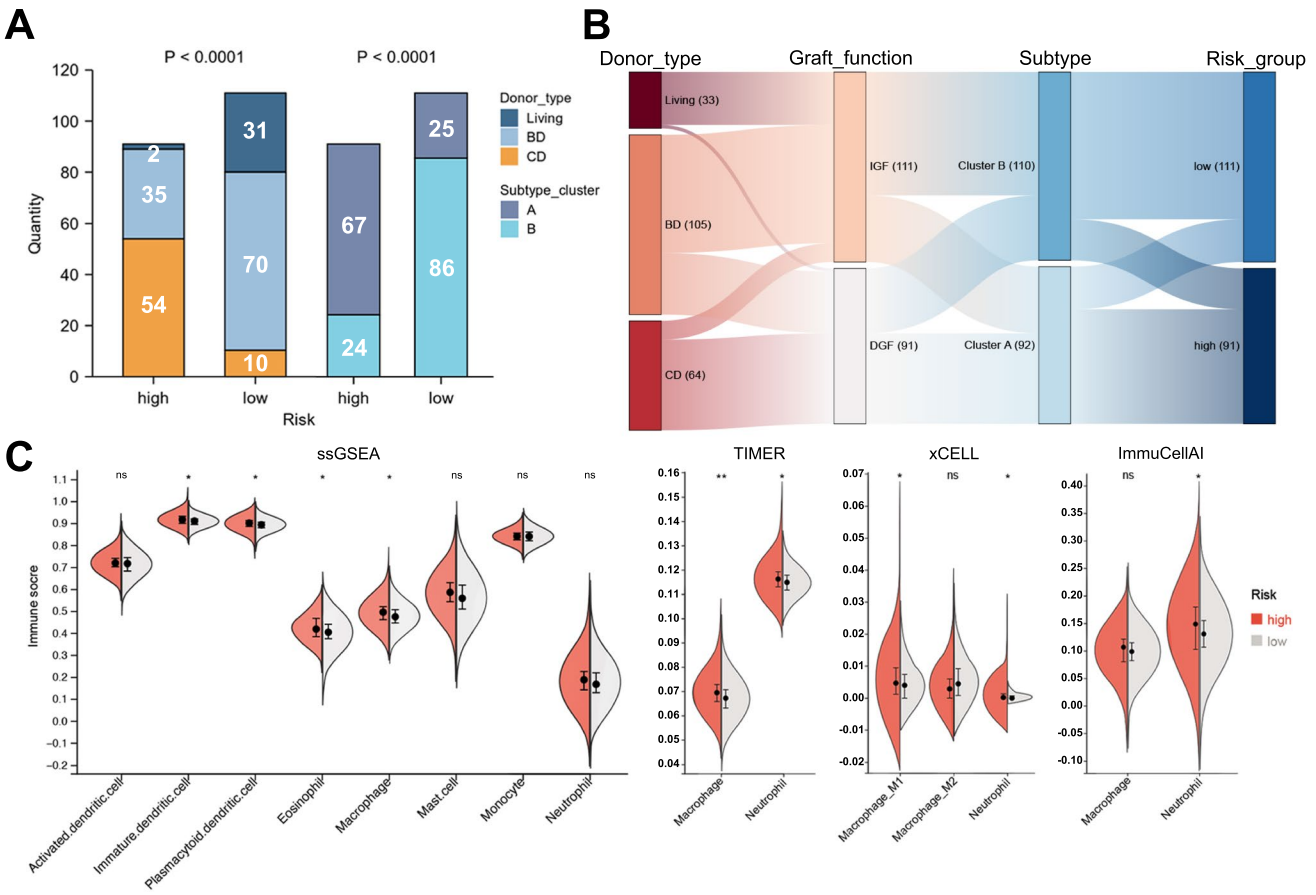

Fig. 8 Clinical correlations and myeloid immune infiltration of the two DGF risk groups and the optimization of the DGF predictive model. **A** Stacked bar charts compared the differences in donor type and IRI subtype between the two groups. **B** Sankey diagram showing the relationships among the donor type, graft function, IRI cluster, and the risk of IRI samples. **C** Myeloid immune infiltration of the two DGF risk groups. BD, brain dead; CD, cardiac dead; DGF, delayed graft function; IGF, immediate graft function. $*p<0.05$; $**p<0.01$; ns, $p\geq0.05$

is an important challenge for a subset of KTx patients that needs to be addressed at the early post-surgical stage. However, while some previous predictive tools have been widely applied, their effectiveness is still limited [20]. Therefore, effective predictive strategies for DGF and graft failure need to be explored. The identification of biomarkers will facilitate the early identification and development of novel drugs targeting DGF to improve the prognosis of KTx. Consensus clustering provided us with two IRI subtypes. Cluster A patients appeared to experience more severe necroptosis and necroinflammation, supported by upregulated DAMPs (ANXA1 and HSP90AA1) as well as decreased NFKBIA expression; furthermore, this cluster was more associated with DGF and DCD donors and had a higher allograft rejection pathway activity. On the other hand, the LASSO regression identified the final candidate NiNRGs for predicting DGF occurrence (ANXA1, HSP90AA1, and NFKBIA) and allograft loss (ANXA1, EGR1, JUN, MYC, and NFKBIA); this helped us to construct different prognostic predictive models for KTx patients by machine learning algorithms. Higher risk scores are associated with a poorer prognosis, including a higher incidence of DGF and shorter graft survival. These results suggested the significance of NiNRGs in the early prediction of graft dysfunction. In high-risk patient groups, breaking the loop between necroinflammation and necroptosis and limiting the infiltration of myeloid immune cells are particularly important to prevent complications and improve graft adaptation. In other words, different management patterns for different subtypes are more conducive to precision medicine. The potential of NiNRG-targeted therapy will be discussed in a later section.

Third stage

After the complications have passed through the preclinical stages and have shown observable clinical signs, the key to management is to stop further deterioration that could lead to graft loss or patient mortality. The

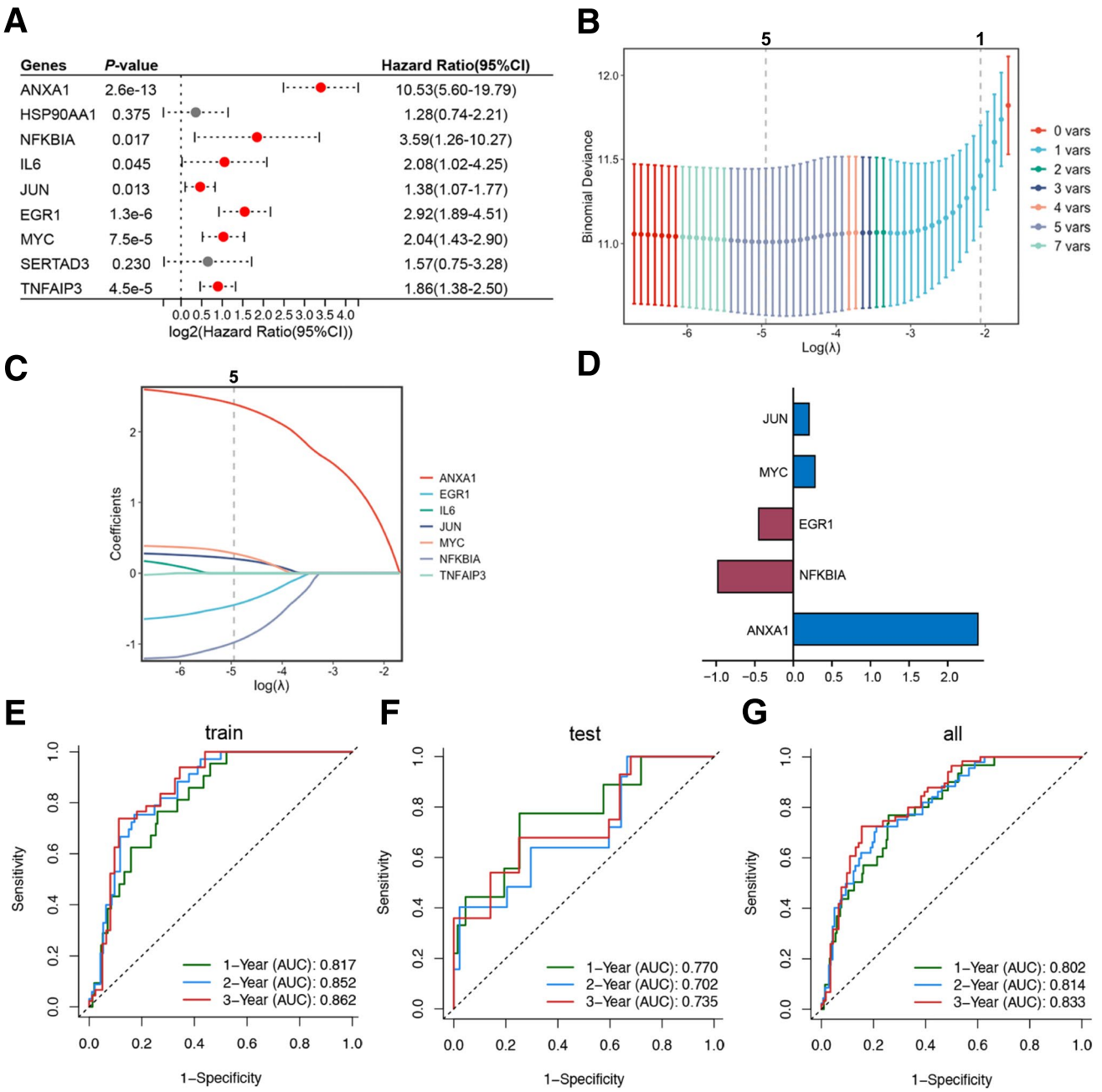

Fig. 9 Establishment and validation of the long-term graft survival predictive model. **A** Forrest plot of univariate Cox regression analysis of the nine DE-NiNRGs. **B**, **C** Five candidate NiNRGs acquired via tenfold cross-validated LASSO regression. **D** Coefficients of the candidate NiNRGs. **E–G** Time-dependent ROC evaluated the performance of the long-term graft survival predictive model in the training set (**E**), the testing set (**F**), and the whole set (**G**). AUC, area under the curve

necroinflammation–necroptosis loop is an important contributor to persistent tubular cell death and renal allograft dysfunction. Potential interventions based on NiNRGs may be beneficial in this phase, but further research is still needed.

Potential of NINRG-targeted treatment

Our pathway annotation results showed that the IL-17 signaling pathway, the TNF signaling pathway, the Toll-like receptor (TLR) signaling pathway, chronic myeloid

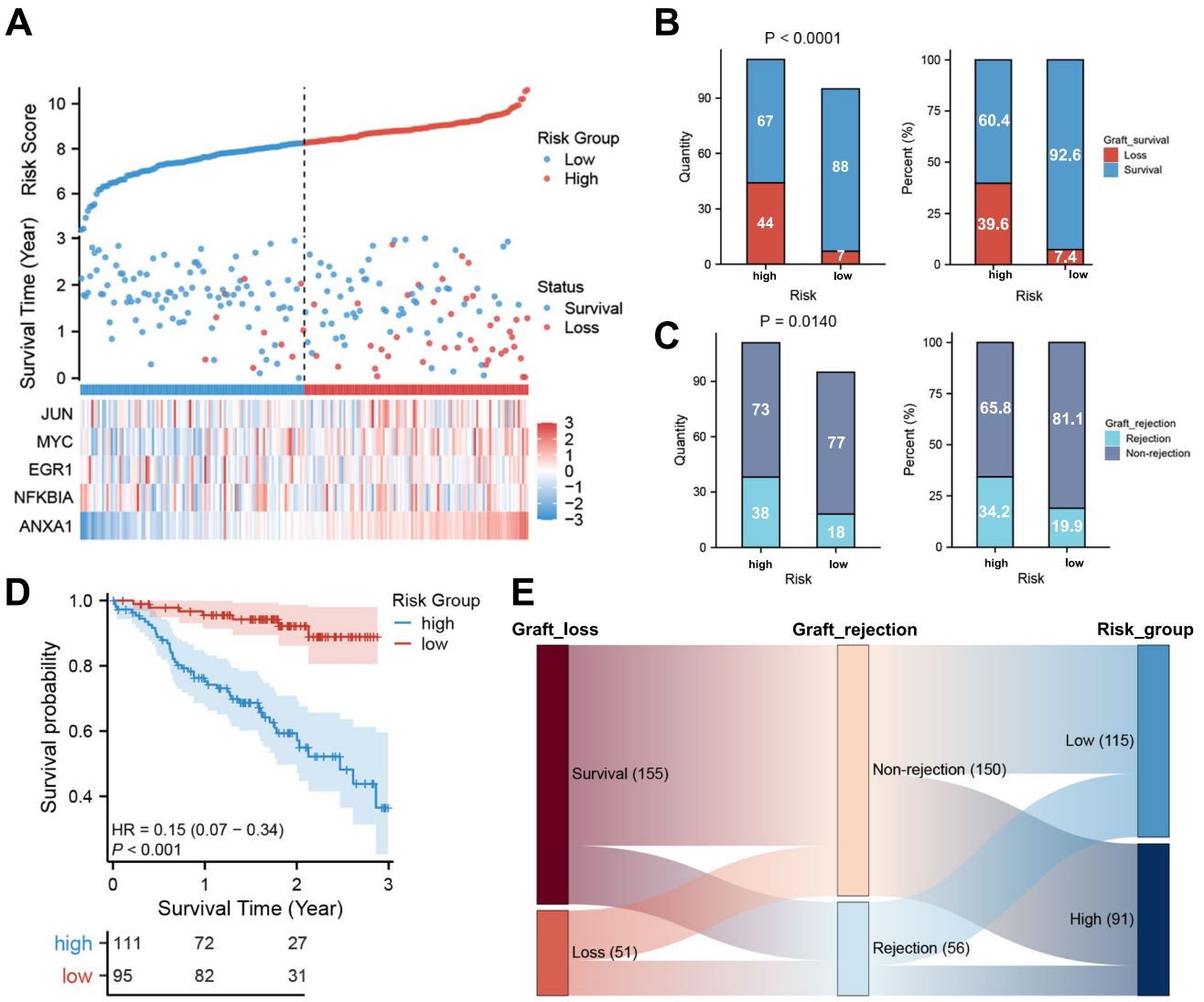

Fig. 10 Clinical correlations of the two long-term risk groups. **A** Risk map of the two long-term risk groups. **B** K–M survival plot shows graft survival over time. **C**, **D** Stacked bar charts compare the differences in the occurrence of graft failure (**C**) and rejection (**D**) between the two long-term risk groups. **E** Relationship among the occurrence of long-term graft failure, graft rejection, and the risk of recipients

interleukins, the PI3K-Akt signaling pathway, the NF-κB signaling pathway, and the JAK-STAT signaling pathway were enriched. In 2012, Linkermann et al. identified that TNF-α-mediated Rip1-dependent post-IRI renal tubular epithelial cell death could be ameliorated by necrostatin-1 (Nec-1); it could also attenuate organ injury and failure, providing initial evidence for necroptosis-related tubular cell loss [65]. TNF-α, commonly elevated after IRI, is considered to be one of the key molecules triggering necroptosis, and the in vitro application of Nec-1 has been found to mitigate the death of murine tubular epithelial cells [34, 65, 70]. Recent reports have demonstrated that the upregulated TWEAK/Fn14 pathway during AKI promotes the release of MCP-1 and IL-6 from bone marrow-derived immune cells and proximal tubular cells via the RIPK3-evoked activation of NF-κB; these inflammatory factors subsequently mediate a necroptosis-dependent second wave of tubular cell death [35]. Indeed, RIPK1 is also implicated in the mediation of TRIF-dependent NF-κB activation via TLR3/4 [71]. In addition, Leng et al. reported that EP3 signaling can also mediate necroinflammatory responses to promote necroptosis, while EP3-deficiency ameliorates IRI-induced AKI by breaking the cycle from necroinflammation to RN [34]. Moreover, IL-6 is capable of activating the JAK-STAT signaling pathway [72, 73], which could downregulate the caspases, including caspase-8 (the switch between necroptosis and apoptosis) [74]. Thus, the suppression of necroinflammation-associated necroptosis may lead to the induction of the apoptotic pathway [33, 34]. Similarly, IL-17 has been reported to contribute to defective autophagy and has been

associated with increased necroptosis [75]; however, there is a dearth of relevant studies on its role in IRI or AKI. The relevance of these pathways also laterally corroborates the activation of necroinflammation-associated necroptotic pathways in the early post-IRI stage. Furthermore, caspase-8 is involved in the switch from RN to pyroptosis when apoptosis and necroptosis are both blocked [76]. We drew an association between this and the recently proposed term, PANoptosis, a distinct form of cell death that integrates pyroptosis, apoptosis, and necroptosis and is regulated by the PANoptosome [77]. Targeting ferroptosis early after IRI can effectively alleviate cell loss, while blocking necroinflammation-associated necroptosis and caspase-8 seems to yield more benefits. With the technological development of engineered extracellular vesicles, targeting these pathways in the kidney will become more feasible [78].

The immunoinfiltration analysis showed a higher proportion of DCs and macrophages in both Cluster A and the high-DGF-risk group; the latter also had a higher neutrophil abundance. In a recent report, Martin-Sanchez et al. confirmed the key role of bone marrow-derived macrophages (BMDMs) and bone marrow DCs (BMDCs) in evoking necroinflammation via RIPK3, although renal tubular epithelial cells are also involved in the release of inflammatory mediators [35]. However, compared to BMDCs, BMDMs are more dominant, as RIPK3 not only increases IL-6 and IL-1β but also MCP-1 [35]. The role of BM-derived cells, especially myeloid cells, has also been emphasized by Leng et al.; EP3 deficiency in myeloid cells and global EP3 deletion have the same ameliorative effect on renal function after IRI [34]. These findings, combined with our results, suggest that macrophages, DCs, and neutrophils may be promising targets.

Limitations

In the PPPM framework, multi-stage and multi-omics prediction is the key to achieving accurate early intervention and treatment [13]. Here, we have mainly explored the contribution of high-throughput sequencing, machine learning, and comprehensive bioinformatics. Future studies need to integrate classical and emerging indicators or biomarkers, pathology, and imaging. With further improvement of the clinical information of KTx patients or in combination with certain laboratory indicators, a nomogram can be constructed to obtain better predictive ability. New studies on necroinflammation and necroptosis are emerging, so the relevant genes and pathways reported in these articles will expand our gene sets. Moreover, while this study focuses primarily on IRI, AKI caused by other factors warrants further exploration. The stability of the prediction model also requires more data to be validated. The results of this study, along with the multicenter permission for obtaining clinical samples, can also guide future experiments.

Conclusions and expert recommendations

In conclusion, NiNRGs were upregulated early in the renal allograft after experiencing IR and are risk factors for subsequent DGF. NiNRG expression was closely associated with the necroinflammatory response, cell death, and graft rejection pathways; the patient group with higher risk scores based on the NiNRGs showed more activated inflammatory responses, especially infiltration of myeloid-derived immune cells. Dependent on late post-KTx biopsies, a high-risk score also suggested a worse prognosis, including a correlation with chronic rejection and shorter graft survival. The predictive models we constructed were capable of assessing KTx prognosis.

Predictive medical approach

Expression of some NiNRGs was upregulated in renal allografts and was associated with poor prognosis in KTx patients. Based on the results of our analysis, we suggested that ANXA1 and HSP90AA1 may be potential biomarkers for predicting DGF in the early post-KTx stages, while NFKBIA was found to be protective against the development of DGF. Excessive upregulation of ANXA1, MYC, and JUN in later stages after KTx may indicate an increased risk of graft loss, whereas NFKBIA and EGR1 had the opposite effect. These NiNRGs could be useful for developing a multi-stage and multi-omics post-KTx PPPM model in the future.

Targeted prevention

Our work focuses on secondary and tertiary prevention of DGF and graft loss. The expression of NiNRGs reflected the prognostic as well as the immunological characteristics of KTx patients. Identification of these markers in the early post-KTx phase and providing effective targeted interventions may be able to prevent the shift from the pre-clinical to the clinical phase of DGF. NiNRGs have also shown their potential in predicting the risk of late graft loss, which is a prerequisite for treatment to avoid further deterioration in those symptomatic patients.

Personalized treatments

Early identification of necroinflammatory-associated necroptosis can contribute to the clustering of patients and assigning risk levels, thus facilitating different management strategies for different subtypes. For high-risk patients, it is particularly important to target NiNRGs to break the vicious

cycle. NiNRG expression may be a marker of excessive infiltration of myeloid immune cells or, alternatively, evidence for the development of personalized immunotherapy. Targeting these genes may be able to improve the efficacy of immunotherapy while alleviating graft dysfunction. On this basis, combining multi-omics diagnostic and therapeutic strategies under the framework of PPPM can enable personalized treatment of post-KTx patients.

Abbreviations AKI: Acute kidney injury; ATN: Acute tubular necrosis; AUC: Area under the curve; BMDC: Bone marrow dendritic cell; BMDM: Bone marrow-derived macrophage; DAMP: Damage-associated molecular pattern; DBD: Donation after brain death; DC: Dendritic cell; DCD: Donation after cardiac death; DEG: Differentially expressed gene; DE-NiNRG: Differentially expressed NiNRG; DGF: Delayed graft function; ESRD: End-stage renal disease; FA: Folic acid; FDR: False detection rate; GEO: Gene Expression Omnibus; GODT: Global Observatory on Donation and Transplantation; GSVA: Gene set variation analysis; HR: Hazard ratio; IGF: Immediate graft function; IRI: Ischemia/reperfusion injury; KEGG: Kyoto Encyclopedia of Genes and Genomes; K–M: Kaplan–Meier; KTx: Kidney transplantation; LASSO: Least absolute shrinkage and selection operator; MSigDB: Molecular Signatures Database;; Nec-1: Necrostatin-1; NiNRG: Necroinflammation-associated necroptosis-related gene; NiRG: Necroinflammation-related gene; NRG: Necroptosis-related gene; PCA: Principal component analysis; PPPM/3PM: Predictive preventive personalized medicine; *R*: Correlation coefficient; RCD: Regulated cell death; RN: Regulated necrosis; ROC: Receiver operating characteristic; ssGSEA: Single-sample gene set enrichment analysis; WHO: World Health Organization

Supplementary Information The online version contains supplementary material available at https://doi.org/10.1007/s13167-023-00320-w.

Acknowledgements The authors would like to express their deepest appreciation to the GEO, GSEA, KEGG, TIMER, xCELL, ImmuCellAI, and Servier Medical Art (https://smart.servier.com/) for their provision of open-access resources, as well as to the editors and reviewers for their invaluable contributions to this work.

Author contribution All authors contributed to the study's conception and design. Material preparation and data collection were performed by Qing Bi, Ji-Yue Wu, and Xue-Meng Qiu. Data analysis was performed by Qing Bi, Ji-Yue Wu, Xue-Meng Qiu, and Yu-Qing Li. The first draft of the manuscript was written by Qing Bi and reviewed by Ji-Yue Wu, Xue-Meng Qiu, Yu-Qing Li, Yu-Yao Yan, and Ze-Jia Sun. The manuscript was supervised and finalized by Ze-Jia Sun and Wei Wang. All authors read and approved the final manuscript.

Funding This research did not receive any specific grant from funding agencies in the public, commercial, or not-for-profit sectors.

Data availability The data supporting the conclusions of this article are available in the article, Supplementary material, and the GEO repository (https://www.ncbi.nlm.nih.gov/geo/). Further inquiries can be directed to the corresponding authors.

Code availability The "Materials and methods" section indicated all analysis methods, software packages, and online tools. Code requirements can be directed to the corresponding authors.

Declarations

Ethics approval Not applicable.

Consent to participate Not applicable.

Consent for publication All authors have approved the final version to be published.

Competing interests The authors declare no competing interests.

References

1. Organ Donation and Transplantation Activities 2021 Report [Internet]. Global Observatory on Donation and Transplantation (GODT); Available from: https://www.transplant-observatory.org/wp-content/uploads/2022/12/2021-data-global-report-1.pdf. Accessed 20 Jan 2023.
2. Organ Donation and Transplantation Activities 2020 Report [Internet]. Global Observatory on Donation and Transplantation (GODT); Available from: https://www.transplant-observatory.org/2020-international-activities-report/. Accessed 20 Jan 2023.
3. Organ Donation and Transplantation Activities 2012 Report [Internet]. Global Observatory on Donation and Transplantation (GODT); Available from: https://www.transplant-observatory.org/download/2012-activity-data/#. Accessed 20 Jan 2023.
4. Mannon RB. Delayed Graft Function: The AKI of Kidney Transplantation. Nephron. 2018;140(2):94–8. https://doi.org/10.1159/000491558.
5. Schroppel B, Legendre C. Delayed kidney graft function: from mechanism to translation. Kidney Int. 2014;86(2):251–8. https://doi.org/10.1038/ki.2014.18.
6. Hall IE, Reese PP, Doshi MD, Weng FL, Schroppel B, Asch WS, et al. Delayed graft function phenotypes and 12-month kidney transplant outcomes. Transplantation. 2017;101(8):1913–23. https://doi.org/10.1097/TP.0000000000001409.
7. Perasaari JP, Kyllonen LE, Salmela KT, Merenmies JM. Pretransplant donor-specific anti-human leukocyte antigen antibodies are associated with high risk of delayed graft function after renal transplantation. Nephrol Dial Transplant. 2016;31(4):672–8. https://doi.org/10.1093/ndt/gfv391.
8. Yarlagadda SG, Coca SG, Garg AX, Doshi M, Poggio E, Marcus RJ, et al. Marked variation in the definition and diagnosis of delayed graft function: a systematic review. Nephrol Dial Transplant. 2008;23(9):2995–3003. https://doi.org/10.1093/ndt/gfn158.
9. Manyalich M, Nelson H, Delmonico FL. The need and opportunity for donation after circulatory death worldwide. Curr Opin Organ Transplant. 2018;23(1):136–41. https://doi.org/10.1097/MOT.0000000000000486.
10. Perez-Saez MJ, Juega J, Zapatero A, Comas J, Tort J, Lauzurica R, et al. Kidney transplant outcomes in elderly recipients with controlled donation after circulatory death or donation after brain death donors: a registry cohort study. Transpl Int. 2021;34(12):2507–14. https://doi.org/10.1111/tri.14141.
11. Li MT, Ramakrishnan A, Yu M, Daniel E, Sandra V, Sanichar N, et al. Effects of delayed graft function on transplant outcomes: a meta-analysis. Transplant Direct. 2023;9(2):e1433. https://doi.org/10.1097/TXD.0000000000001433.
12. Yarlagadda SG, Coca SG, Formica RN Jr, Poggio ED, Parikh CR. Association between delayed graft function and allograft and patient survival: a systematic review and meta-analysis. Nephrol Dial Transplant. 2009;24(3):1039–47. https://doi.org/10.1093/ndt/gfn667.
13. Golubnitschaja O, Baban B, Boniolo G, Wang W, Bubnov R, Kapalla M, et al. Medicine in the early twenty-first century: paradigm and anticipation - EPMA position paper 2016. EPMA J. 2016;7(1):23. https://doi.org/10.1186/s13167-016-0072-4.

14. Golubnitschaja O, Liskova A, Koklesova L, Samec M, Biringer K, Busselberg D, et al. Caution, "normal" BMI: health risks associated with potentially masked individual underweight-EPMA Position Paper 2021. EPMA J. 2021;12(3):243–64. https://doi.org/10.1007/s13167-021-00251-4.
15. Koklesova L, Mazurakova A, Samec M, Biringer K, Samuel SM, Busselberg D, et al. Homocysteine metabolism as the target for predictive medical approach, disease prevention, prognosis, and treatments tailored to the person. EPMA J. 2021;12(4):477–505. https://doi.org/10.1007/s13167-021-00263-0.
16. Golubnitschaja O, Potuznik P, Polivka J Jr, Pesta M, Kaverina O, Pieper CC, et al. Ischemic stroke of unclear aetiology: a case-by-case analysis and call for a multi-professional predictive, preventive and personalised approach. EPMA J. 2022;13(4):535–45. https://doi.org/10.1007/s13167-022-00307-z.
17. Kubatka P, Mazurakova A, Samec M, Koklesova L, Zhai K, Al-Ishaq R, et al. Flavonoids against non-physiologic inflammation attributed to cancer initiation, development, and progression-3PM pathways. EPMA J. 2021;12(4):559–87. https://doi.org/10.1007/s13167-021-00257-y.
18. Ma X, Wang Y, Wu H, Li F, Feng X, Xie Y, et al. Periodontal health related-inflammatory and metabolic profiles of patients with end-stage renal disease: potential strategy for predictive, preventive, and personalized medicine. EPMA J. 2021;12(2):117–28. https://doi.org/10.1007/s13167-021-00239-0.
19. Sena CM, Goncalves L, Seica R. Methods to evaluate vascular function: a crucial approach towards predictive, preventive, and personalised medicine. EPMA J. 2022;13(2):209–35. https://doi.org/10.1007/s13167-022-00280-7.
20. Ietto G, Guzzetti L, Baglieri CS, Raveglia V, Zani E, Benedetti F, et al. Predictive models for the functional recovery of transplanted kidney. Transplant Proc. 2021;53(10):2873–8. https://doi.org/10.1016/j.transproceed.2021.08.053.
21. Lai C, Yee SY, Ying T, Chadban S. Biomarkers as diagnostic tests for delayed graft function in kidney transplantation. Transpl Int. 2021;34(12):2431–41. https://doi.org/10.1111/tri.14132.
22. Quaglia M, Merlotti G, Guglielmetti G, Castellano G, Cantaluppi V. Recent advances on biomarkers of early and late kidney graft dysfunction. Int J Mol Sci. 2020;21(15) https://doi.org/10.3390/ijms21155404.
23. Golubnitschaja O, Watson ID, Topic E, Sandberg S, Ferrari M, Costigliola V. Position paper of the EPMA and EFLM: a global vision of the consolidated promotion of an integrative medical approach to advance health care. EPMA J. 2013;4(1):12. https://doi.org/10.1186/1878-5085-4-12.
24. Ponticelli C. Ischaemia-reperfusion injury: a major protagonist in kidney transplantation. Nephrol Dial Transplant. 2014;29(6):1134–40. https://doi.org/10.1093/ndt/gft488.
25 Zhao H, Alam A, Soo AP, George AJT, Ma D. Ischemia-reperfusion injury reduces long term renal graft survival: mechanism and beyond. EBioMedicine. 2018;28:31–42. https://doi.org/10.1016/j.ebiom.2018.01.025.
26. Granata S, Votrico V, Spadaccino F, Catalano V, Netti GS, Ranieri E, et al. Oxidative stress and ischemia/reperfusion injury in kidney transplantation: focus on ferroptosis, mitophagy and new antioxidants. Antioxidants (Basel). 2022;11(4); https://doi.org/10.3390/antiox11040769.
27. Han SJ, Lee HT. Mechanisms and therapeutic targets of ischemic acute kidney injury. Kidney Res Clin Pract. 2019;38(4):427–40. https://doi.org/10.23876/j.krcp.19.062.
28. Zhang F, Li Y, Wu J, Zhang J, Cao P, Sun Z, et al. The role of extracellular traps in ischemia reperfusion injury. Front Immunol. 2022;13:1022380. https://doi.org/10.3389/fimmu.2022.1022380.
29. Wu Z, Deng J, Zhou H, Tan W, Lin L, Yang J. Programmed cell death in sepsis associated acute kidney injury. Front Med (Lausanne). 2022;9:883028. https://doi.org/10.3389/fmed.2022.883028.
30. Sun Z, Wu J, Bi Q, Wang W. Exosomal lncRNA TUG1 derived from human urine-derived stem cells attenuates renal ischemia/reperfusion injury by interacting with SRSF1 to regulate ASCL4-mediated ferroptosis. Stem Cell Res Ther. 2022;13(1):297. https://doi.org/10.1186/s13287-022-02986-x.
31. Belavgeni A, Meyer C, Stumpf J, Hugo C, Linkermann A. Ferroptosis and necroptosis in the kidney. Cell Chem Biol. 2020;27(4):448–62. https://doi.org/10.1016/j.chembiol.2020.03.016.
32. Martin-Sanchez D, Ruiz-Andres O, Poveda J, Carrasco S, Cannata-Ortiz P, Sanchez-Nino MD, et al. Ferroptosis, but not necroptosis, is important in nephrotoxic folic acid-induced AKI. J Am Soc Nephrol. 2017;28(1):218–29. https://doi.org/10.1681/ASN.2015121376.
33. Martin-Sanchez D, Fontecha-Barriuso M, Carrasco S, Sanchez-Nino MD, Massenhausen AV, Linkermann A, et al. TWEAK and RIPK1 mediate a second wave of cell death during AKI. Proc Natl Acad Sci U S A. 2018;115(16):4182–7. https://doi.org/10.1073/pnas.1716578115.
34. Leng J, Zhao W, Guo J, Yu G, Zhu G, Ge J, et al. E-prostanoid 3 receptor deficiency on myeloid cells protects against ischemic acute kidney injury via breaking the auto-amplification loop of necroinflammation. Kidney Int. 2022. https://doi.org/10.1016/j.kint.2022.08.019.
35. Martin-Sanchez D, Guerrero-Mauvecin J, Fontecha-Barriuso M, Mendez-Barbero N, Saiz ML, Lopez-Diaz AM, et al. Bone marrow-derived RIPK3 mediates kidney inflammation in acute kidney injury. J Am Soc Nephrol. 2022;33(2):357–73. https://doi.org/10.1681/ASN.2021030383.
36. Muller T, Dewitz C, Schmitz J, Schroder AS, Brasen JH, Stockwell BR, et al. Necroptosis and ferroptosis are alternative cell death pathways that operate in acute kidney failure. Cell Mol Life Sci. 2017;74(19):3631–45. https://doi.org/10.1007/s00018-017-2547-4.
37. Khoury MK, Gupta K, Franco SR, Liu B. Necroptosis in the pathophysiology of disease. Am J Pathol. 2020;190(2):272–85. https://doi.org/10.1016/j.ajpath.2019.10.012.
38. Gong Y, Fan Z, Luo G, Yang C, Huang Q, Fan K, et al. The role of necroptosis in cancer biology and therapy. Mol Cancer. 2019;18(1):100. https://doi.org/10.1186/s12943-019-1029-8.
39. Stranneheim H, Wedell A. Exome and genome sequencing: a revolution for the discovery and diagnosis of monogenic disorders. J Intern Med. 2016;279(1):3–15. https://doi.org/10.1111/joim.12399.
40. Greener JG, Kandathil SM, Moffat L, Jones DT. A guide to machine learning for biologists. Nat Rev Mol Cell Biol. 2022;23(1):40–55. https://doi.org/10.1038/s41580-021-00407-0.
41 Barrett T, Wilhite SE, Ledoux P, Evangelista C, Kim IF, Tomashevsky M, et al. NCBI GEO: archive for functional genomics data sets–update. Nucleic Acids Res. 2013;41(Database issue):D991-5. https://doi.org/10.1093/nar/gks1193.
42. Damman J, Bloks VW, Daha MR, van der Most PJ, Sanjabi B, van der Vlies P, et al. Hypoxia and complement-and-coagulation pathways in the deceased organ donor as the major target for intervention to improve renal allograft outcome. Transplantation. 2015;99(6):1293–300. https://doi.org/10.1097/TP.0000000000000500.
43. McGuinness D, Mohammed S, Monaghan L, Wilson PA, Kingsmore DB, Shapter O, et al. A molecular signature for delayed graft function. Aging Cell. 2018;17(5):12825. https://doi.org/10.1111/acel.12825.
44. Cippa PE, Sun B, Liu J, Chen L, Naesens M, McMahon AP. Transcriptional trajectories of human kidney injury progression. JCI Insight. 2018;3(22). https://doi.org/10.1172/jci.insight.123151
45. Kusaka M, Kuroyanagi Y, Ichino M, Sasaki H, Maruyama T, Hayakawa K, et al. Serum tissue inhibitor of metalloproteinases

1 (TIMP-1) predicts organ recovery from delayed graft function after kidney transplantation from donors after cardiac death. Cell Transplant. 2010;19(6):723–9. https://doi.org/10.3727/096368910X508825.
46. Einecke G, Reeve J, Sis B, Mengel M, Hidalgo L, Famulski KS, et al. A molecular classifier for predicting future graft loss in late kidney transplant biopsies. J Clin Invest. 2010;120(6):1862–72. https://doi.org/10.1172/JCI41789.
47. Stelzer G, Rosen N, Plaschkes I, Zimmerman S, Twik M, Fishilevich S, et al. The GeneCards Suite: from gene data mining to disease genome sequence analyses. Curr Protoc Bioinformatics. 2016;54:1 30 1–1 3 https://doi.org/10.1002/cpbi.5.
48. Chen T, Zhang H, Liu Y, Liu YX, Huang L. EVenn: Easy to create repeatable and editable Venn diagrams and Venn networks online. J Genet Genomics. 2021;48(9):863–6. https://doi.org/10.1016/j.jgg.2021.07.007.
49. Szklarczyk D, Gable AL, Nastou KC, Lyon D, Kirsch R, Pyysalo S, et al. The STRING database in 2021: customizable protein-protein networks, and functional characterization of user-uploaded gene/measurement sets. Nucleic Acids Res. 2021;49(D1):D605–12. https://doi.org/10.1093/nar/gkaa1074.
50 Wu T, Hu E, Xu S, Chen M, Guo P, Dai Z, et al. clusterProfiler 4.0: A universal enrichment tool for interpreting omics data. Innovation (Camb). 2021;2(3):100141. https://doi.org/10.1016/j.xinn.2021.100141.
51. Kanehisa M, Furumichi M, Sato Y, Kawashima M, Ishiguro-Watanabe M. KEGG for taxonomy-based analysis of pathways and genomes. Nucleic Acids Res. 2022. https://doi.org/10.1093/nar/gkac963.
52. Liberzon A, Birger C, Thorvaldsdottir H, Ghandi M, Mesirov JP, Tamayo P. The Molecular Signatures Database (MSigDB) hallmark gene set collection. Cell Syst. 2015;1(6):417–25. https://doi.org/10.1016/j.cels.2015.12.004.
53. Li B, Severson E, Pignon JC, Zhao H, Li T, Novak J, et al. Comprehensive analyses of tumor immunity: implications for cancer immunotherapy. Genome Biol. 2016;17(1):174. https://doi.org/10.1186/s13059-016-1028-7.
54. Aran D, Hu Z, Butte AJ. xCell: digitally portraying the tissue cellular heterogeneity landscape. Genome Biol. 2017;18(1):220. https://doi.org/10.1186/s13059-017-1349-1.
55. Miao YR, Zhang Q, Lei Q, Luo M, Xie GY, Wang H, et al. ImmuCellAI: a unique method for comprehensive T-cell subsets abundance prediction and its application in cancer immunotherapy. Adv Sci (Weinh). 2020;7(7):1902880. https://doi.org/10.1002/advs.201902880.
56. Wilkerson MD, Hayes DN. ConsensusClusterPlus: a class discovery tool with confidence assessments and item tracking. Bioinformatics. 2010;26(12):1572–3. https://doi.org/10.1093/bioinformatics/btq170.
57. Friedman J, Hastie T, Tibshirani R. Regularization paths for generalized linear models via coordinate descent. J Stat Softw. 2010;33(1):1–22.
58. Zens TJ, Danobeitia JS, Leverson G, Chlebeck PJ, Zitur LJ, Redfield RR, et al. The impact of kidney donor profile index on delayed graft function and transplant outcomes: a single-center analysis. Clin Transplant. 2018;32(3):13190. https://doi.org/10.1111/ctr.13190.
59. Shao MJ, Ye QF, Ming YZ, She XG, Liu H, Ye SJ, et al. Risk factors for delayed graft function in cardiac death donor renal transplants. Chin Med J (Engl). 2012;125(21):3782–5.
60. Galluzzi L, Vitale I, Aaronson SA, Abrams JM, Adam D, Agostinis P, et al. Molecular mechanisms of cell death: recommendations of the Nomenclature Committee on Cell Death 2018. Cell Death Differ. 2018;25(3):486–541. https://doi.org/10.1038/s41418-017-0012-4.
61. Zhang M, Song R, Liu Y, Yi Z, Meng X, Zhang J, et al. Calcium-overload-mediated tumor therapy by calcium peroxide nanoparticles. Chem. 2019;5(8):2171–82. https://doi.org/10.1016/j.chempr.2019.06.003.
62. Tsvetkov P, Coy S, Petrova B, Dreishpoon M, Verma A, Abdusamad M, et al. Copper induces cell death by targeting lipoylated TCA cycle proteins. Science. 2022;375(6586):1254–61. https://doi.org/10.1126/science.abf0529.
63. Schumer M, Colombel MC, Sawczuk IS, Gobe G, Connor J, O'Toole KM, et al. Morphologic, biochemical, and molecular evidence of apoptosis during the reperfusion phase after brief periods of renal ischemia. Am J Pathol. 1992;140(4):831–8.
64. Skouta R, Dixon SJ, Wang J, Dunn DE, Orman M, Shimada K, et al. Ferrostatins inhibit oxidative lipid damage and cell death in diverse disease models. J Am Chem Soc. 2014;136(12):4551–6. https://doi.org/10.1021/ja411006a.
65. Linkermann A, Brasen JH, Himmerkus N, Liu S, Huber TB, Kunzendorf U, et al. Rip1 (receptor-interacting protein kinase 1) mediates necroptosis and contributes to renal ischemia/reperfusion injury. Kidney Int. 2012;81(8):751–61. https://doi.org/10.1038/ki.2011.450.
66. Proneth B, Conrad M. Ferroptosis and necroinflammation, a yet poorly explored link. Cell Death Differ. 2019;26(1):14–24. https://doi.org/10.1038/s41418-018-0173-9.
67 Kang ZY, Liu C, Liu W, Li DH. Effect of C1q-binding donor-specific anti-HLA antibodies on the clinical outcomes of patients after renal transplantation: a systematic review and meta-analysis. Transpl Immunol. 2022;72:101566. https://doi.org/10.1016/j.trim.2022.101566.
68. Ngamvichchukorn T, Ruengorn C, Noppakun K, Thavorn K, Hutton B, Sood MM, et al. Association between pretransplant dialysis modality and kidney transplant outcomes: a systematic review and meta-analysis. JAMA Netw Open. 2022;5(10):e2237580. https://doi.org/10.1001/jamanetworkopen.2022.37580.
69. Shin JH, Koo EH, Ha SH, Park JH, Jang HR, Lee JE, et al. The impact of slow graft function on graft outcome is comparable to delayed graft function in deceased donor kidney transplantation. Int Urol Nephrol. 2016;48(3):431–9. https://doi.org/10.1007/s11255-015-1163-1.
70. Yang Z, Wang Y, Zhang Y, He X, Zhong CQ, Ni H, et al. RIP3 targets pyruvate dehydrogenase complex to increase aerobic respiration in TNF-induced necroptosis. Nat Cell Biol. 2018;20(2):186–97. https://doi.org/10.1038/s41556-017-0022-y.
71. Udawatte DJ, Lang DM, Currier JR, Medin CL, Rothman AL. Dengue virus downregulates TNFR1- and TLR3-stimulated NF-kappaB activation by targeting RIPK1. Front Cell Infect Microbiol. 2022;12:926036. https://doi.org/10.3389/fcimb.2022.926036.
72. Zhang HX, Yang PL, Li EM, Xu LY. STAT3beta, a distinct isoform from STAT3. Int J Biochem Cell Biol. 2019;110:130–9. https://doi.org/10.1016/j.biocel.2019.02.006.
73. Fathi N, Rashidi G, Khodadadi A, Shahi S, Sharifi S. STAT3 and apoptosis challenges in cancer. Int J Biol Macromol. 2018;117:993–1001. https://doi.org/10.1016/j.ijbiomac.2018.05.121.
74. Tan M, Rong Y, Su Q, Chen Y. Artesunate induces apoptosis via inhibition of STAT3 in THP-1 cells. Leuk Res. 2017;62:98–103. https://doi.org/10.1016/j.leukres.2017.09.022.
75. Lee SY, Lee AR, Choi JW, Lee CR, Cho KH, Lee JH, et al. IL-17 induces autophagy dysfunction to promote inflammatory cell death and fibrosis in keloid fibroblasts via the STAT3 and HIF-1alpha dependent signaling pathways. Front Immunol. 2022;13:888719. https://doi.org/10.3389/fimmu.2022.888719.
76. Wu YH, Mo ST, Chen IT, Hsieh FY, Hsieh SL, Zhang J, et al. Caspase-8 inactivation drives autophagy-dependent inflammasome

activation in myeloid cells. Sci Adv. 2022;8(45):eabn9912. https://doi.org/10.1126/sciadv.abn9912.
77 Wang Y, Kanneganti TD. From pyroptosis, apoptosis and necroptosis to PANoptosis: a mechanistic compendium of programmed cell death pathways. Comput Struct Biotechnol J. 2021;19:4641–57. https://doi.org/10.1016/j.csbj.2021.07.038.
78 Tang TT, Wang B, Lv LL, Dong Z, Liu BC. Extracellular vesicles for renal therapeutics: state of the art and future perspective. J Control Release. 2022;349:32–50. https://doi.org/10.1016/j.jconrel.2022.06.049.

Authors and Affiliations

Qing Bi[1,2] · Ji-Yue Wu[1,2] · Xue-Meng Qiu[1,2,3] · Yu-Qing Li[1,2] · Yu-Yao Yan[4] · Ze-Jia Sun[1,2] · Wei Wang[1,2]

✉ Ze-Jia Sun
mnwkszj5076@163.com

✉ Wei Wang
weiwang0920@163.com

1 Department of Urology, Beijing Chao-Yang Hospital, Capital Medical University, Beijing, China

2 Institute of Urology, Capital Medical University, Beijing, China

3 Third Clinical Medical College, Capital Medical University, Beijing, China

4 Department of Anesthesiology, Beijing Obstetrics and Gynecology Hospital, Capital Medical University, Beijing, China